INVESTIGATION OF ENERGY TRANSFER IN SAMARIUM DOPED CALCIUM TUNGSTATE CRYSTALS USING TIME RESOLVED SITE SELECTION SPECTROSCOPY

By

WILLIAM BRYAN SMITH

Bachelor of Science

Kansas State University

Manhattan, Kansas

1975

Submitted to the Faculty of the Graduate College
of the Oklahoma State University
in partial fulfillment of the requirements
for the Degree of
DOCTOR OF PHILOSOPHY
December, 1980

INVESTIGATION OF ENERGY TRANSFER IN SAMARIUM DOPED CALCIUM TUNGSTATE CRYSTALS USING TIME RESOLVED SITE SELECTION SPECTROSCOPY

Thesis Approved:

Richard C. Powell
Thesis Adviser

Jeff Brunes

Wm. G. Rockley

Larry E. Halliburton

Norman N. Durham
Dean of the Graduate College

ACKNOWLEDGMENTS

I would like to acknowledge the contribution and support of my parents above all. The accomplishments represented by this document are as much the results of their work as mine.

In addition I would like to acknowledge the moral support provided by Brigid during the long, final stages of this work. I hope I am able to repay in kind. To Dick Powell, I offer my appreciation for his help, which extends far beyond his aid in this project. My thanks also to Mark Rockley, a superb educator from whom I learned so much during our short collaboration. For their assistance in the final stages of manuscript preparation I thank Dhiraj Sardar and Dee Behrens. This work was supported in part by a grant from the U. S. Army Research Office.

TABLE OF CONTENTS

LIST OF TABLES

LIST OF FIGURES

CHAPTER I

INTRODUCTION

Purpose of Investigation

The spectra of the rare earth ions are complicated and in general are composed of many sharp lines (1). Much work has been done on characterizing the interactions between rare earth ions (2-8). Many of the rare earths have applications as potential or proven laser materials, in particular Nd^{3+} used in high power lasers. Sm^{3+} has had an important use for years as a commercial phosphor material. Calcium tungstate itself has had important applications as X-ray intensifier phosphor in addition to being a laser host material.

The purpose of this investigation is to continue and to expand upon work begun earlier in characterizing energy transfer between samarium ions in $CaWO_4$ using the powerful technique of time resolved spectroscopy (9). To that end, work will concentrate on determination of the quenching and energy transfer mechanisms in the temperature range $10^{o}K$-$200^{o}K$.

Apparatus and Samples

Samples of Sm^{3+} doped $CaWO_4$ were obtained from Airtron, Inc., in concentrations of 0.01, 0.1, 0.5, 1.0, 2.0, and 5.0 percent by weight. Charge compensation was achieved by addition of equal amounts of Na^{+} which, like samarium, is known to substitute for Ca^{2+} in the

scheelite structure (see Figure 1). Samples were cut and polished from boules of good optical quality that were grown along the crystal a-axis.

A diagram of the experimental set up is shown in Figure 2. The exitation source consists of a tunable dye laser pumped by a pulsed nitrogen laser. The National Research Group nitrogen N_2 laser, operated at 30 Hz has an output at 3371 Å of approximately 350 kw with a pulse duration of about 10 ns. The output is focused into the dye cell of a Systems Science and Software model DL-8 tunable dye laser tuned to give an output line width of 0.5 Å.

Samples were mounted on the cold finger of an Air Products model CS202 Displex Cryogenic Refrigerator. This is a closed cycle helium refrigerator with an attached heater element allowing continuous variation of sample temperature between 10°K and room temperature.

To study the effects of uniaxial stress on lifetimes and spectra, a sample holder consisting of a flat base and a hydraulically driven piston was used. The apparatus was constructed in the OSU Physics Machine Shop. A temperature of 77°K was maintained by emersing in the meter long piston assembly in liquid nitrogen.

Sample emission was analyzed with a Spex model 1704 1-meter Czerny-Turner spectrometer with a 5000 Å blaze grating, giving a dispersion of 4 Å/mm. Slits were opened to give an operating resolution of 0.6 Å for the analysis of fluorescence spectra. Signals were detected with a cooled RCA C31034 photomultiplier tube mounted on the spectrometer.

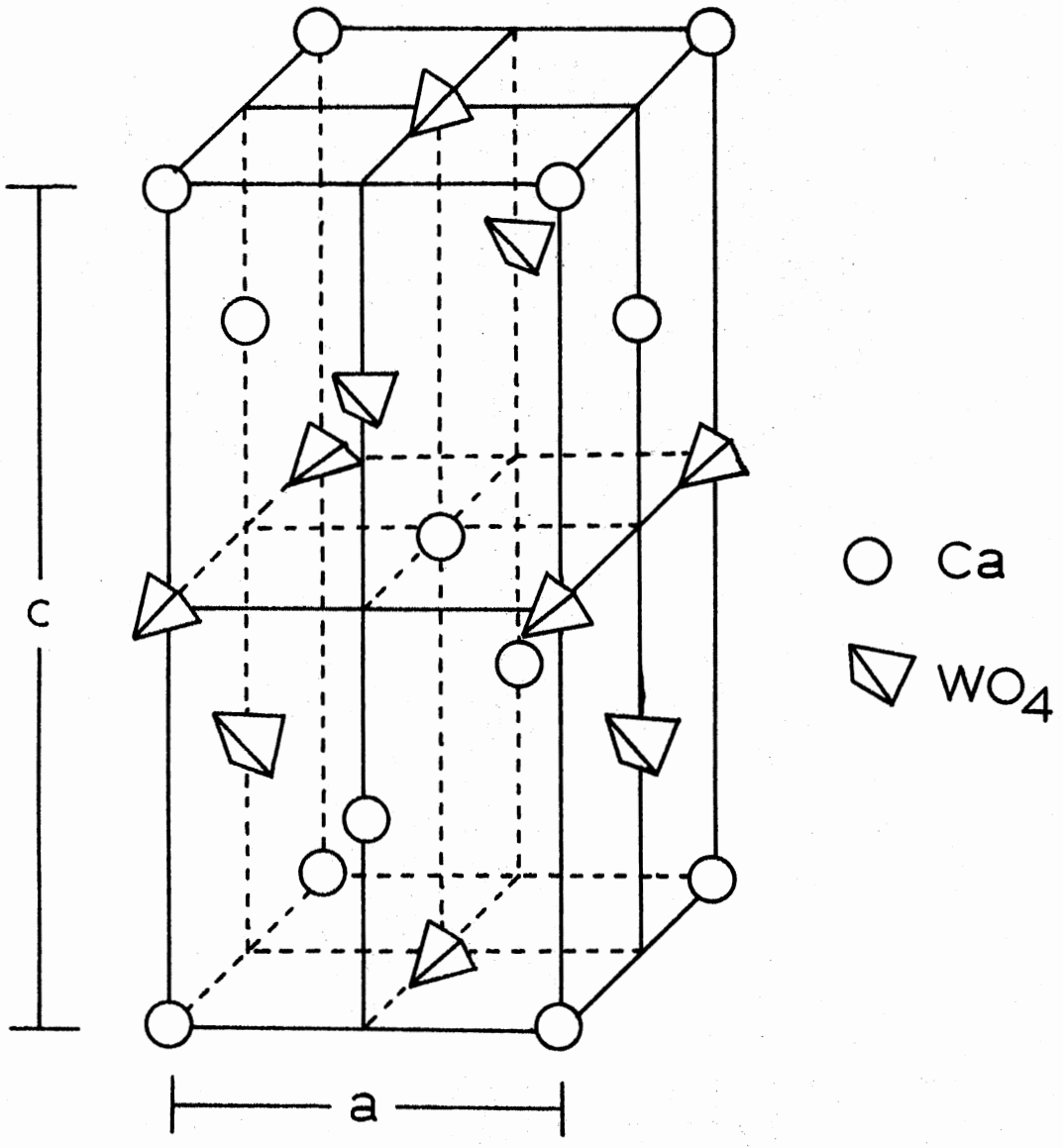

Figure 1. Scheelite Structure of $CaWO_4$

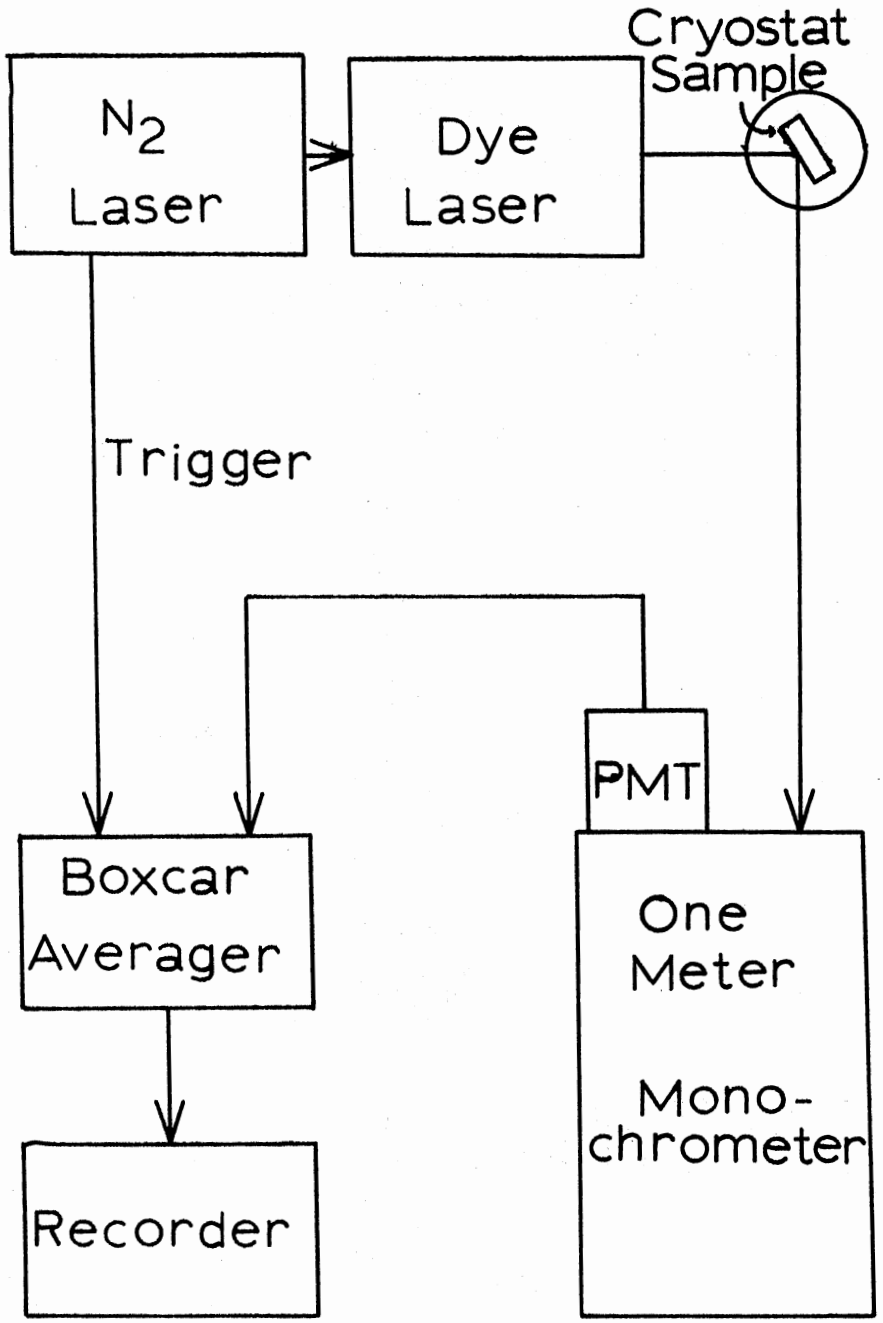

Figure 2. TRS Apparatus

Output signals from the photomultiplier tube were processed with a Princeton Applied Research model 162 Boxcar Averager with a model 165 Gated Integrator and recorded on a strip chart recorder.

Review of Previous Work

A knowledge of the energy levels resulting from the five 4f electrons in Sm^{3+} is essential in interpreting the luminescence spectra in crystals. Work on the lower lying levels has been done (10)(11) and the most recent work (12) indicates the lowest lying metastable state from which luminescence occurs is the $^4F_{5/2}$ level. Luminescence in the visable regions of the spectra is due to transitions to the ^6H_J levels, the ground state being the $^6H_{5/2}$ level. The ^4F-^6H transitions are forbidden in the free ion and hence their oscillator strengths in crystals are small ($\sim 10^{-6}$). Figures 3 and 4 show an absorption spectra of Sm^{3+} in $CaWO_4$ and an emission spectra showing transitions from $^4F_{5/2}$ to the lowest lying ^6H manifolds. Figure 5 shows an emperical energy level diagram of Sm^{3+} in $CaWO_4$ for the lowest lying states.

The number of weak fluorescence lines observed in the spectra of Sm^{3+} in $CaWO_4$ has made analysis of the spectra difficult. Many extraneous lines appear which may be due to a number of sources. Vibronic transitions may be responsible for satellite lines appearing at an energy lower than the major line by an amount equal to the phonon frequency. A large number of phonon frequencys in $CaWO_4$ have been observed in the range of 100 cm^{-1} to 450 cm^{-1} (13)(14). An important source of additional lines is the presence of nonequivalent sites for the samarium ions. Charge compensation for the samples used

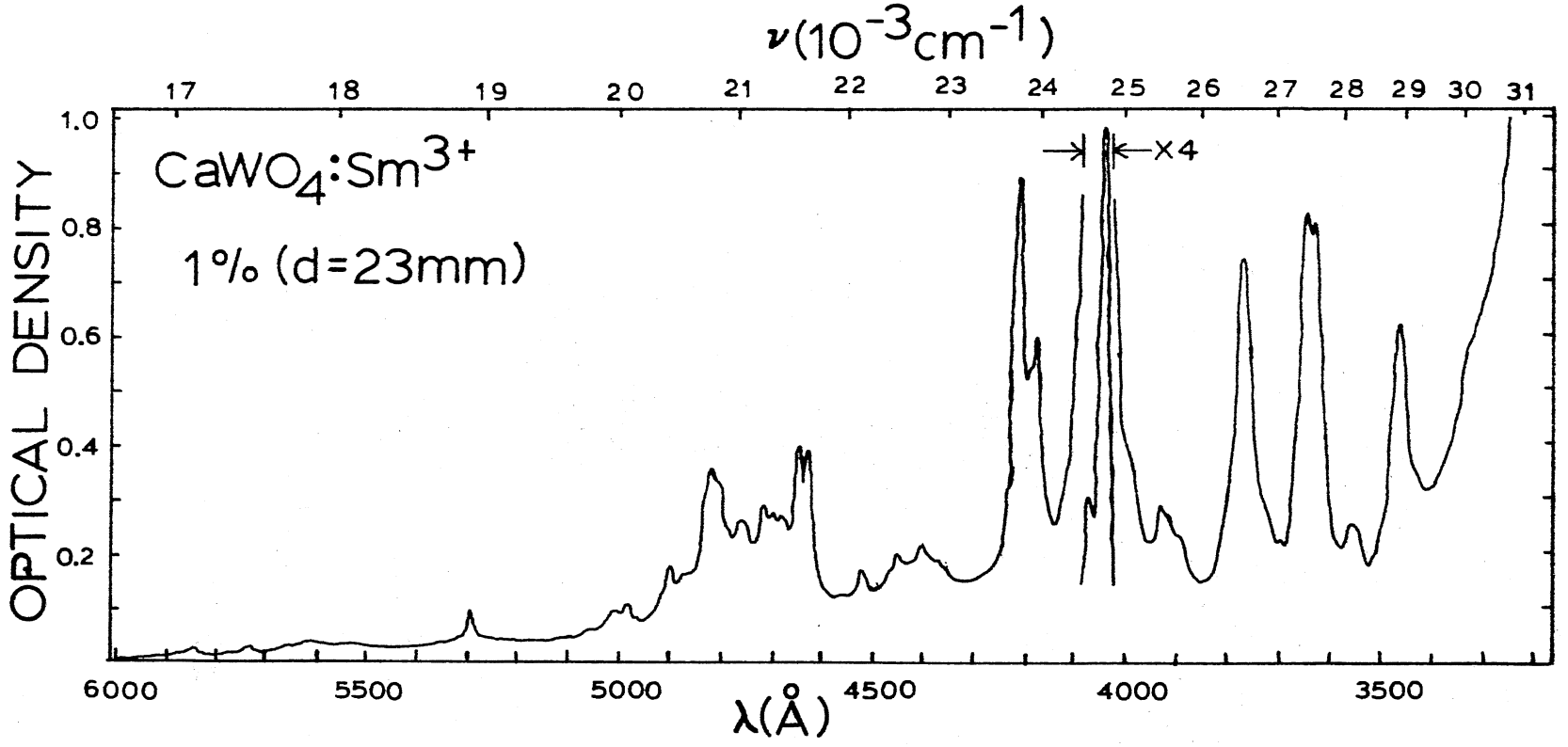

Figure 3. Absorption Spectra of $CaWO_4:Sm^{3+}$ 1.0%

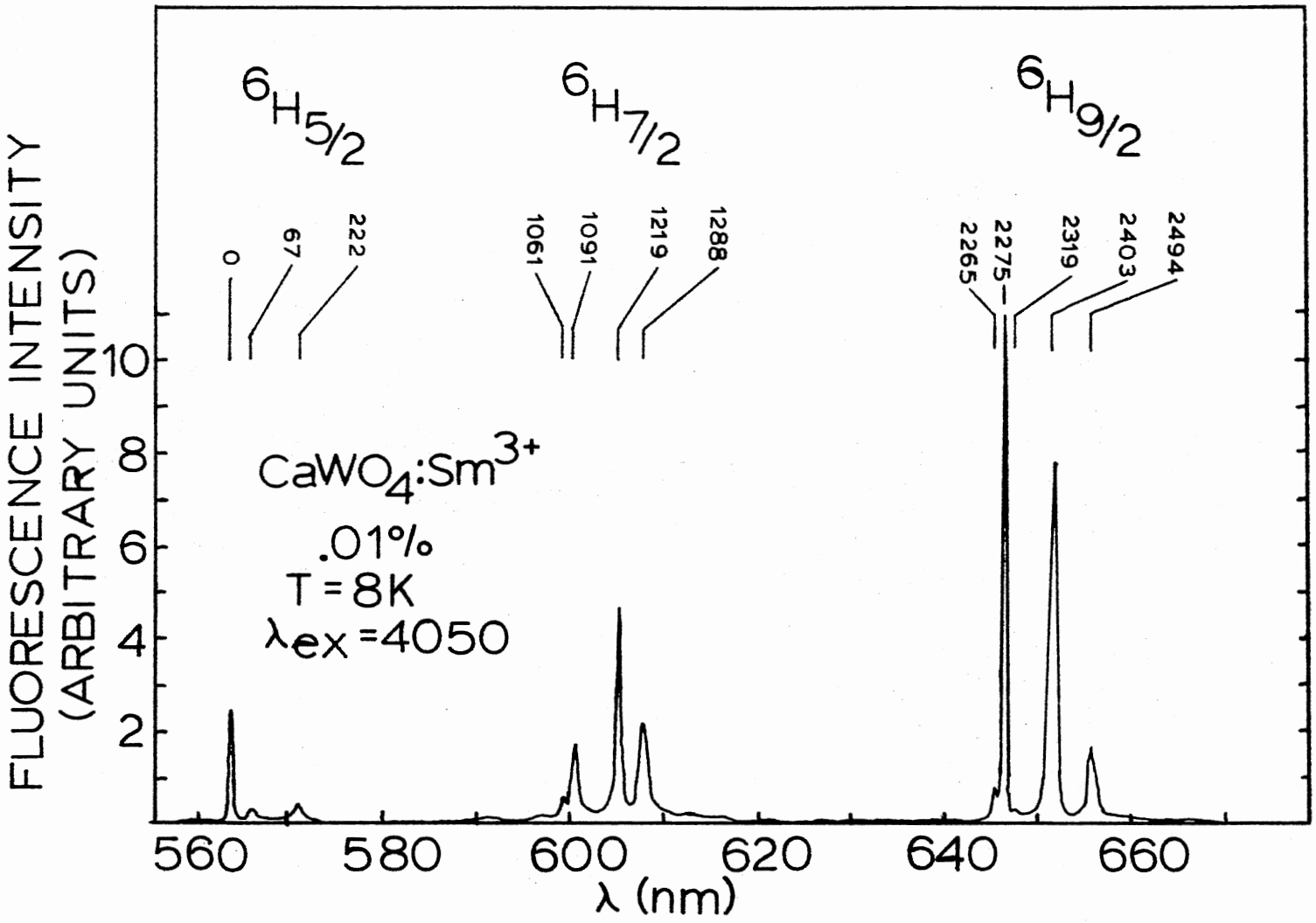

Figure 4. Fluorescence Spectra of $CaWO_4:Sm^{3+}$ .01% for 4050 Å Excitation at 8°K

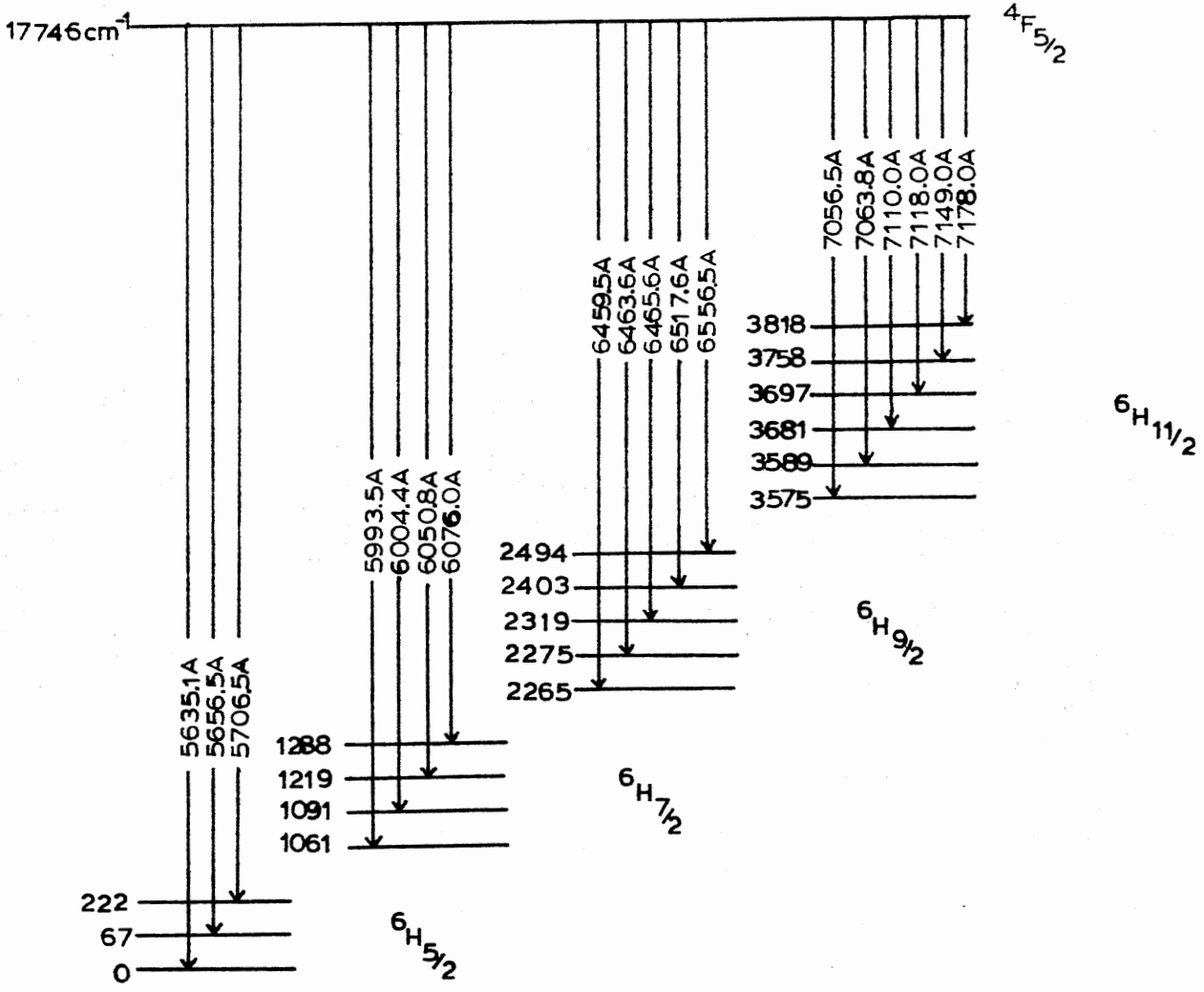

Figure 5. Emperical Energy Level Diagram of Sm^{3+} in Calcium Tungstate

in this study is accomplished by addition of equal amounts of Na^+ to the lattice. Electron spin resonance results indicate most charge compensation is nonlocal (15) but some local charge compensation does exist.

Previous work by Hsu and Powell has shown the existence of non-equivalent crystal field sites in the $CaWO_4:Sm^{3+}$ system based on the examination of exitation and emission spectra (9). Figure 6 shows the exitation spectra obtained when fluorescence is monitored at 6464 Å and 6451 Å. Figure 7 is the fluorescence spectra resulting from exitation into the narrow 4020 exitation peak and at 4050 Å. The exitation at 4020 Å includes essentially all the features seen for 4050 Å exitation in addition to numerous new lines. The interpretation is that the new features are the result of exitation of a higher energy site via the 4020 Å exitation peak.

Of particular interest in this study is the fluoresence peak at 5632 Å and fluorescence from the higher energy site at 5615 Å. If the fluorescence spectra is monitored in this region as a function of time, a change in relative integrated intensitys between the lines corresponding to the two sites is seen in Figure 8. The behavior between 5 μs and 100 μs shows a decrease in integrated intensity of the 5615 Å line and its satellites and a simultaneous relative increase in the integrated intensity of the 5632 Å line and its satellites indicating energy transfer. Hsu and Powell saw no energy transfer between these line groupings at low temperature but did see transfer between the satellites and their respective major lines, also seen clearly in Figure 8. They determined that the interaction here was of electric quadrupole-quadrupole strength. The onset of transfer between the

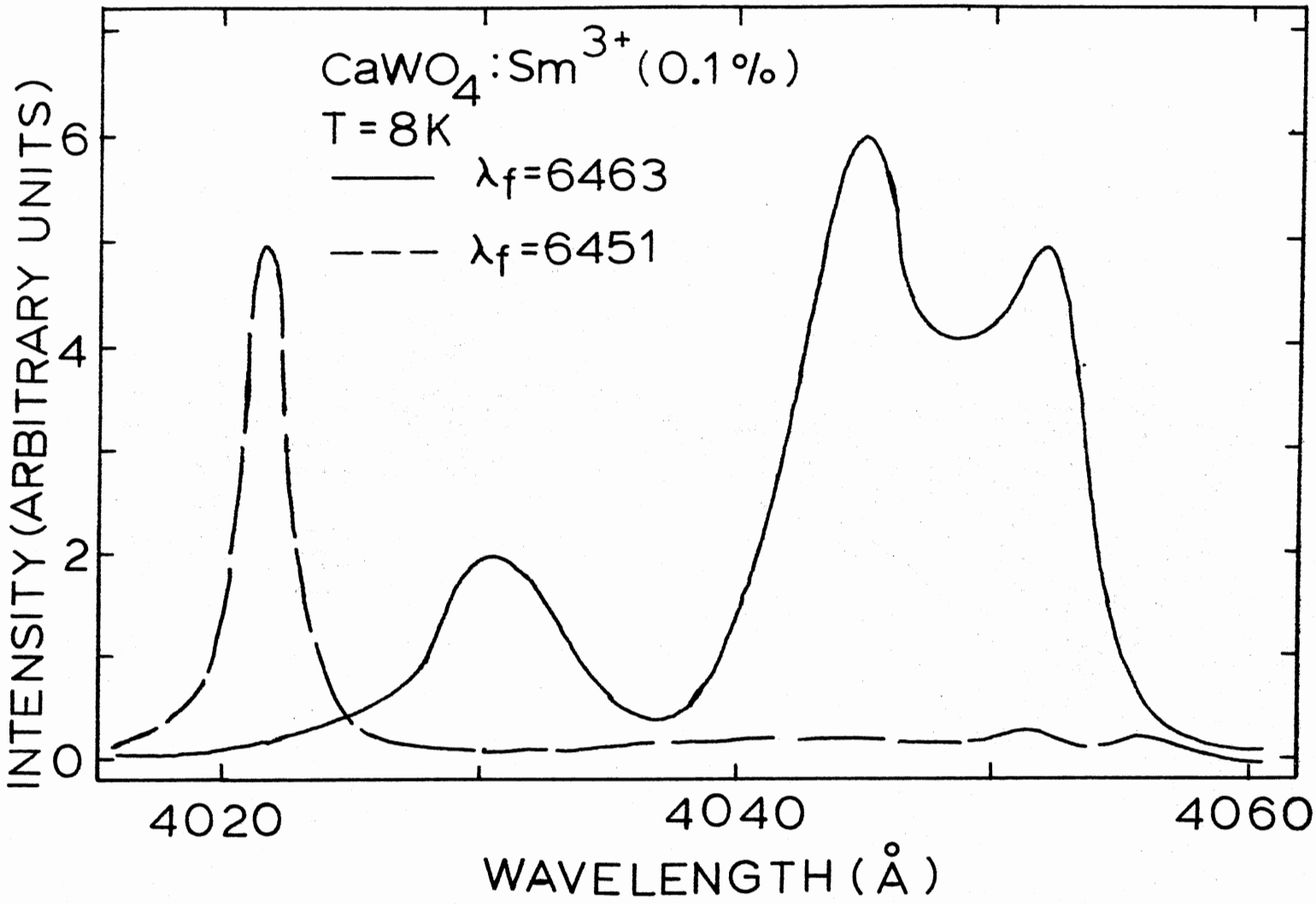

Figure 6. Laser Excitation

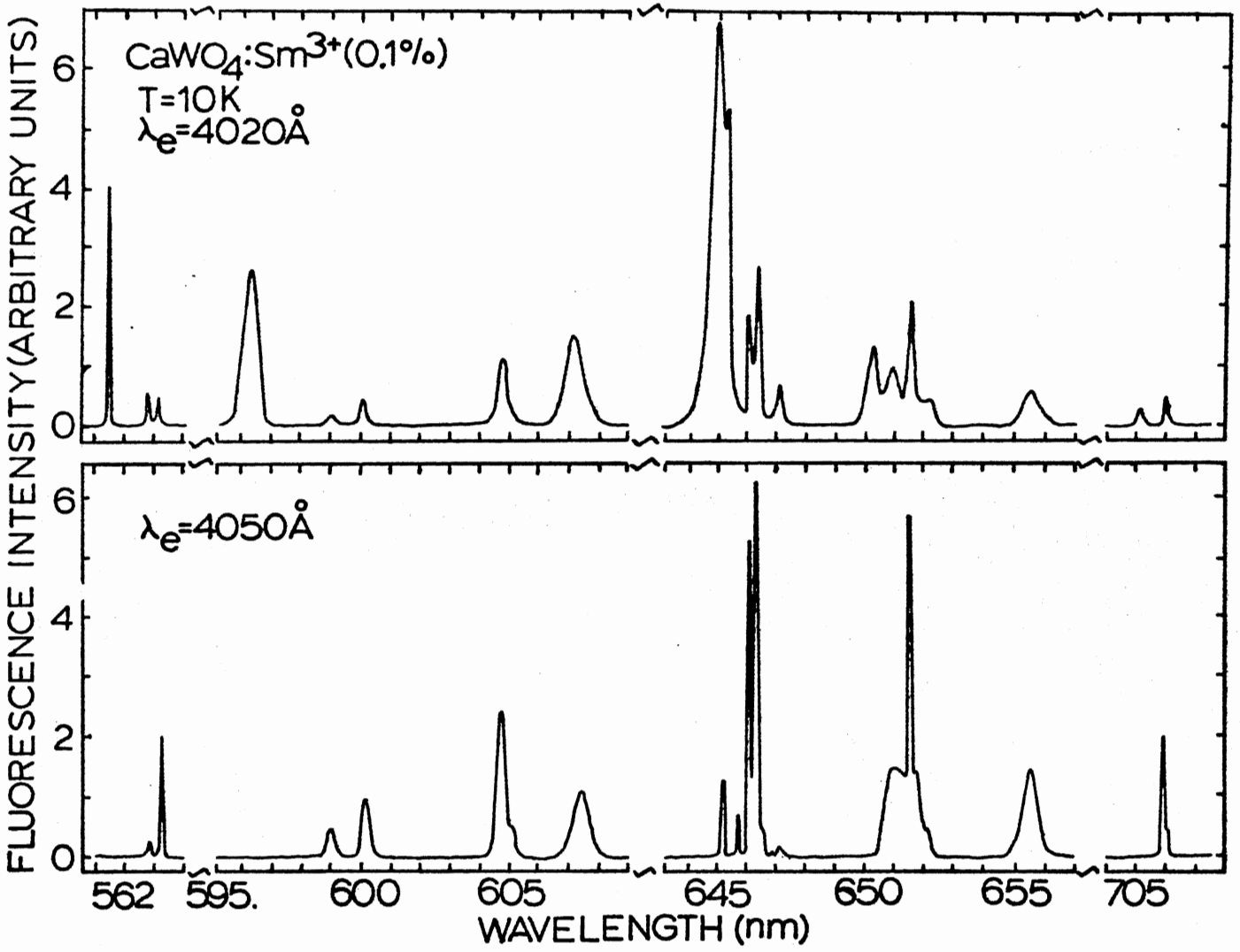

Figure 7. Laser Excited Fluorescence Spectra

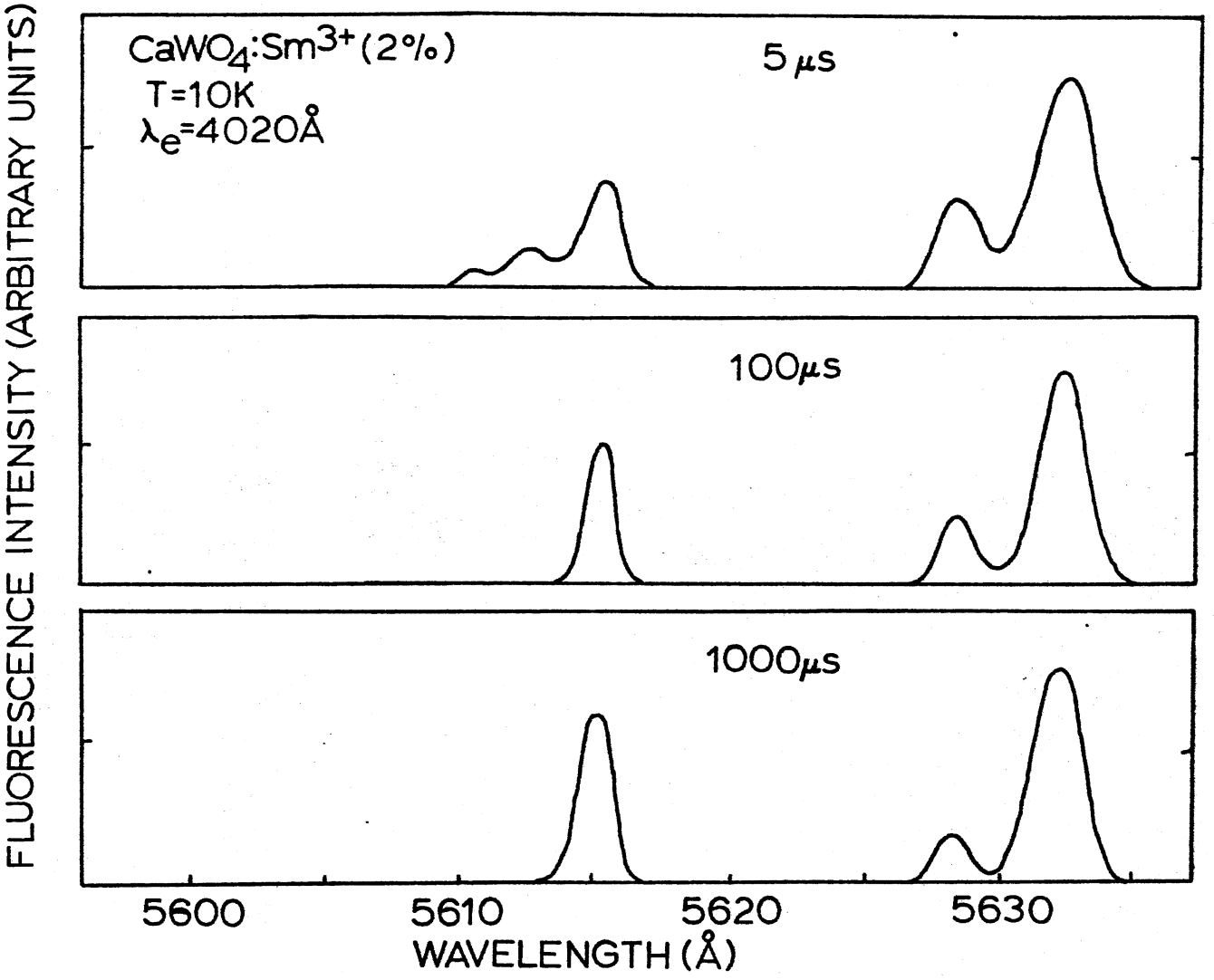

Figure 8. Fluorescence of $^{4}F_{5/2}$ to $^{6}H_{5/2}$ Transition at Different Times After Pulse

major lines was seen by Hsu and Powell only at higher temperatures. Another interesting feature is the apparent change, between 100 μs and 1000 μs, of transfer of energy from the 5632 Å line back to the 5615 Å line. This will be seen later to be due to the lifetime of the 5615 Å line being larger than that of the 5632 Å line, resulting in a more rapid decrease in the intensity of the 5632 line. This effect can be seen because of the rapid decrease of the time dependent transfer rate due to its exchange interaction strength. This will be discussed later.

Information on the nature of the lattice in the vicinity of Sm^{3+} is of great importance insofar as the mechanism of interaction seen in this study appears to be the exchange interaction, which has a range limited to a few nearest neighbors in distance (16). Even if super exchange, involving anion intermediaries, occurs the effective distances are still very small (17). There is evidence to indicate the satellite lines observed at energys slightly higher than the major line may be due to sites having first, second or third nearest neighbor compensation ions. Mims and Gillan (18) have studied electron spin resonance spectra of $CaWO_4:Ce^{3+}$ and have identified a number of sites which they attribute to charge compensators located at first, second, and third nearest neighbors.

There is evidence that samarium ions distort the lattice locally. There has been important work done on characterizing host sensitized energy transfer in $CaWO_4:Sm^{3+}$ (19) (20) and recent work indicates that the red edge of the $CaWO_4$ absorption band selectively excites tungstate ions nearby to samarium ions (21), which indicates the red tail of

the absorption band is due to the perturbations caused by the samarium ions.

As mentioned earlier, the exchange interaction operates effectively over small distances and if other multipole interactions are present, the exchange interaction contributes little to energy transfer if the distribution of sites is uniform. Previous work suggested that for the case of trivalent rare earths, where the electric dipole transition is forbidden, the electric quadrupole-quadrupole interaction governs energy transfer (22). Kushida's (7) work deals with concentration effects on the order of influence of the interactions. It is clear though that exchange interaction cannot be expected to play a dominant role in energy transfer between impurity ions in a lightly doped host unless clustering is occurring.

Summary

This investigation used the technique of time resolved spectroscopy to investigate Sm^{3+}-Sm^{3+} energy transfer in a $CaWO_4$ host. Various concentrations were used, ranging from 0.01% samarium to 5.0% samarium by weight.

Results indicate that at low temperature, energy is transferred via a single step exchange interaction from sensitizer lying in one crystal field site to activators lying in a crystal field site with a smaller transition energy. A model which features a time dependent transfer rate without any back transfer, and different intrinsic lifetimes for sensitizer and activator was the only model found which could explain the data. The fluorescent emission line observed is thought to correspond to the $^4F_{5/2}$-$^6H_{5/2}$ transition in the free ion.

The energy difference between the sensitizer and activator transitions due to site differences is measured to be 54 cm^{-1}.

At temperatures above $50^{o}K$ the transfer becomes predominantly multistep in nature and the model which best accounts for the observed behavior involves both forward and back transfer rates which are constant in time. The temperature dependence of the ratio of the forward to back transfer rates is explained by assuming a sensitizer-sensitizer migration of energy which involves a one site resonant two phonon assisted process. The sensitizer-activator and activator-sensitizer step is assumed to be a one phonon assisted process. The resonant two phonon assisted process requires the existance of an additional electronic level which results of analysis predict to be located 106 cm^{-1} above the lowest lying state in the $^{4}F_{5/2}$ manifold. Steady state emission spectra at room temperature taken by Treadaway (23) support the prediction.

A series of lifetime measurements, at $10^{o}K$ for each sample, illustrate the onset of concentration quenching at 0.5% samarium. The functional dependence of the quenching rate on concentration indicates the mechanism responsible for the observed quenching is exchange interaction.

The exchange interaction can be a dominant mechanism at small distances but owing to the exponental decrease of its strength with distance, it is not expected to play an important role in energy transfer at longer distances if other multipole interactions are active. Since other multipole interactions do occur, it seems that the narrow line exitation used may be preferentially exciting clusters of samarium ions.

CHAPTER II

THEORY

The Exchange Interaction

A number of mechanisms can be responsible for energy transfer in crystals. Among them are the electric dipole-dipole, electric dipole-quadrupole, and electric quadrupole-quadrupole interaction, and the exchange interaction. These transfer mechanisms give rise to different distance dependences of the transfer rate for a given sensitizer activator pair. The three electric multipole interactions have distance dependences of R^{-q} where q = 6, 8, and 10 for dipole-dipole, dipole-quadrupole, and quadrupole-quadrupole, respectively. The exchange interaction has a distance dependence of e^{-R}, where R is the sensitizer activator distance.

The early development of multipole energy transfer is found in the classic works of Förster (24) (25). Dexter (16) continued with a theoretical study of energy transfer which considered the exchange interaction. To obtain the time dependences of transfer rates, which are described by a single ion-ion pair separation, the solution to the rate equation must be averaged over all of relevant space by assuming a uniform distribution of ions. This averaging has been done for multipole interactions (25) (26) and Inokuti and Hirayama (27) have applied the technique to the exchange interaction. It is the latter work which is summarized here.

The rate constant for energy transfer by the exchange mechanism has been derived by Dexter (16):

$$\omega(R) = \frac{2\pi}{\hbar} K^2 \, I \, \exp^{(-2R/L)}$$

with

$$I = \int f_s(E) F_A(E) dE$$

where L is an effective average Bohr radius for the sensitizer and activator ions, K is a constant with dimensions of energy, and I is the overlap integral of the normalized sensitizer emission spectra and the normalized activator absorption spectra. The parameter L is taken to be approximately 1 $\mathring{A}$ which is close to one half the tungsten-oxygen separation (.9 $\mathring{A}$). It is convenient to rewrite the rate constant in the form

$$\omega(R) = \beta_s^o \exp\left[\gamma(1-R/R_o)\right]$$

where

$$\gamma = \frac{2R_o}{L} \qquad \text{and} \qquad \beta_s^o e^{\gamma} = \frac{2\pi}{\hbar} K^2 \, I$$

Here R_o refers to the critical transfer distance at which for a single sensitizer activator pair the energy transfer rate is equal to the rate of spontaneous deactivation, β_s^o.

Consider a set of excited sensitizers with a particular configuration of neighboring activators. Denote the population of this set of excited sensitizers as $n_c(t)$. If the set c is initially populated by a delta function excitation at t=0, the population at any subsequent time is given by $n_c(t) = n_c(0) \exp\left[-(\beta_s^o+\omega_c)t\right]$ where $n_c(0)$ is the

initial population of t=0, β_s^o is the sum of the intrinsic decay rate of the sensitizer in the absence of activators and the rate of quenching, and ω_c is the sum of the transfer rates between the sensitizer and all neighboring activators, N_a, separated by distance R_i.

$$\omega_c = \sum_{i=1}^{N_a} \omega(R_i)$$

then

$$n_c(t) = n_c(0) \exp(-\beta_s^o t) \prod_{i=1}^{N_a} \exp(-\omega(R_i)t)$$

To find the average n(t) of all sets of sensitizers configurations we add $n_c(t)$ for all sensitizer configurations and divide by the total number of configurations.

$$n(t) \alpha \frac{\prod_{i=1}^{N_a} \exp(-\omega^1(R_i)t) + \prod_{i=1}^{N_a} \exp(-\omega^2(R_i)t) + \ldots + \prod_{i=1}^{N_a} \exp(-\omega^{N_s}(R_i)t)}{N_s}$$

where N_s is the total number of excited sensitizers.

Alternately, a uniform spacial distribution of sensitizers and activators can be assumed. The probability of finding an activator at a distance R is then given by

$$PdR = \frac{4\pi R^2 dR}{V}$$

where V is the crystal volume.

Then

$$n(t) \alpha \int_0^{R_v} \prod_{i=1}^{N_a} \exp(-\omega(R_i)t) P_i dR_i$$

or

$$n(t)\alpha\left[\int_o^{R_v} \exp\ (-\omega(R)t)PdR\right]^{N_a}$$

Finally

$$n(t) = n(0)\ \exp\ (-\beta_s^o t)\left[\frac{4\pi}{V}\int_o^{R_v} \exp\left[(-\beta_s^o t)\ \exp[\gamma(1-R/R_o)]\right] R^2 dR\right]^{N_a}$$

To do the integral the substitutions are made.

$$Z = \beta_s^o t e^{\gamma}$$

$$y_v = \exp\ (-\gamma R_v/R_o)$$

$$n(t) = n(0)\ \exp\ (-\beta_s^o t)\left[3\gamma^{-3}\left(\frac{R_o}{R_v}\right)^3 \int_{y_v}^1 y^{-1}e^{-zy}(\ell n\ y)^2 dy\right]^{N_a} \qquad (1)$$

integrating by parts

$$\int_{y_v}^1 y^{-1}e^{-zy}(\ell n\ y)^2 dy = -\frac{1}{3}\ e^{-zy_v}(\ell n\ y_v)^3 + \frac{2}{3}\left\{\int_o^1 e^{-zy}(\ell n\ y)^3 dy - \int_o^{y_v} e^{-zy}(\ell n\ y)^3 dy\right\}$$

and for small y_v

$$\int_{y_v}^1 y^{-1}e^{-zy}(\ell n\ y)^2 dy = \frac{1}{3}(\ell n\ y_v)^3 - \frac{1}{3}\ g(z) + O\ [y_v(\ell n\ y_v)^3] \qquad (2)$$

where

$$g(z) = -z \int_0^1 e^{-zy} (\ell n\ y)^3 dy \tag{3}$$

substituting back into (1).

$$n(t) = n(o)\ \exp\ (-\beta_s^o t) \left[1 - \gamma^{-3} (R_o/R_v)^3 g(z) \right]^{N_a}$$

$$n(t) = n(o)\ \exp\ (-\beta_s^o t)\ \exp \left[-\gamma^{-3} (R_o/R_v)^3 N_a g(z) \right]$$

$$n(t) = n(o)\ \exp \left[(-\beta_s^o t) - \gamma^{-3} (c/c_o) g(z) \right] \tag{4}$$

where c is the activator concentration and c_o is called the critical concentration.

$$c_o = \frac{3}{4\pi R_o^3}$$

Expansion of the exponential in (3) allows the function to be integrated term by term to give

$$g(z) = 6z \sum_{m=0}^{\infty} \frac{(-z)^m}{m!\,(m+1)^4} \tag{5}$$

For z > 10 it is more convenient to rewrite

$$g(z) = \int_0^Z e^{-u} \ell n \left(\frac{u}{Z}\right)^3 du \qquad \text{where} \qquad u = zy$$

which results in

$$g(z) = (\ell n\ z)^3 + h_1(\ell n\ z)^2 + h_2\ (\ell n\ z) + h_3 \qquad (6)$$

$$h_1 = 1.7316$$

$$h_2 = 5.9343$$

$$h_3 = 5.4449$$

where the h values are related to derivatives of the polygamma function for large z.

Low Temperature Energy Transfer Model

Throughout this development it has been assumed that the period of lattice vibrations is large compared to the time required for the energy transfer to occur. Each energy transfer process can be considered to occur at a fixed sensitizer-activator distance if this is the case. A second assumption is that the distribution of activators and sensitizers is uniform and random. This is obviously not the case due to the discrete nature of the latice in the vicinity of any given sensitizer. Nor is the distribution random if there exists any clustering of samarium ions, within the lattice. There is indeed evidence suggesting that there may be clustering of Sm ions within $CaWO_4$.

Consider now the model represented by Figure 9 in which n(t) is the population of excited sensitizers, m(t) is the population of excited activators, W and W′ are the respective pump rates, β_{sq} and β_{aq} the respective quenching rates and $\omega_{sa}(t)$ is the energy transfer rate.

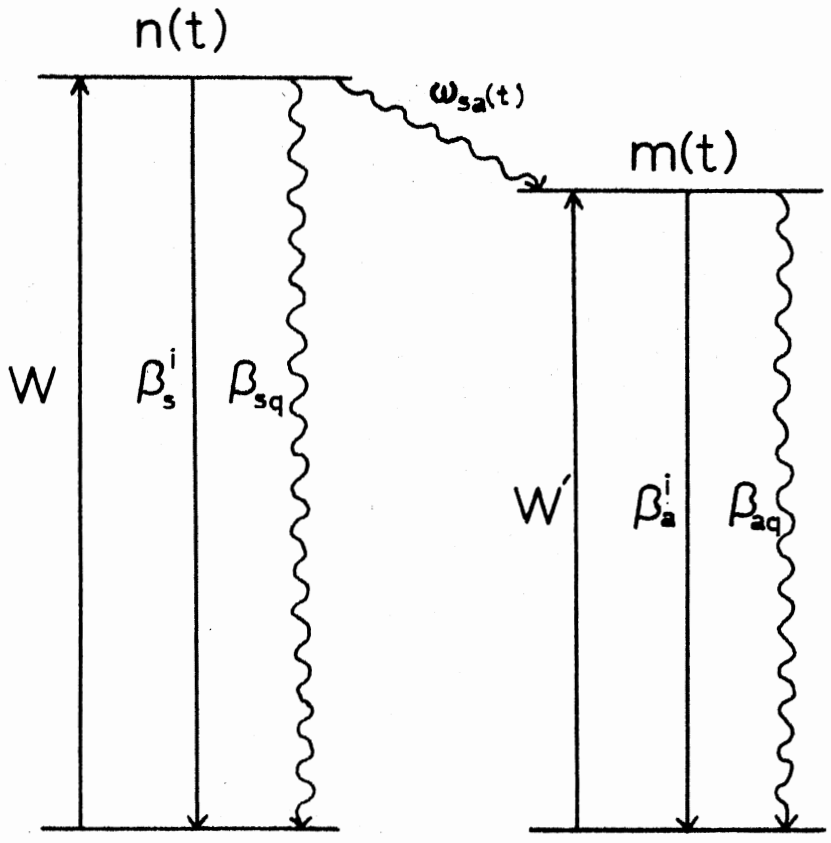

Figure 9. Two Level Model for Low Temperature Energy Transfer

A rate equation can now be written for the system of activators. Following the development for sensitizers, we have for a set of activators with a given configuration of sensitizers.

$$\frac{dm_c(t)}{dt} = \omega_{sa}(R)n(t) - \beta_a^o m_c(t)$$

$$m_c(t) = m_c(o)e^{-\beta_a^o t} + \frac{\omega_{sa} n(o)}{\beta_a^o - \beta_s^o - \omega_{sa}} \left(e^{-(\beta_s^o + \omega_{sa})t} - e^{-\beta_a^o t} \right)$$

An attempt to apply the sort of spacial averaging technique used previously will prove unsuccessful due to problems encountered with $\omega_{sa}(R)$ outside the exponential. As an approximation, assume that the term

$$e^{-[\beta_s^o t + \omega_{sa}(R)]t},$$

having the same functional form as the solution of the sensitizer rate equation, will give rise to a term of the form

$$e^{-(\beta_s^o t + \gamma^{-3}(c/c_o)g(z))}$$

after equal averaging. Then,

$$m(t) = m(o)e^{-\beta_a^o t} + \frac{\langle\omega\rangle n(o)}{\beta_a^o - \beta_s^o - \langle\omega\rangle} \left(e^{-[\beta_s^o t + \gamma^{-3}(c/c_o)g(z)]} - e^{-\beta_a^o t} \right) \quad (7)$$

The problem remains of justifying the choice of an expression for $\langle\omega\rangle$, the result of the term $\omega_{sa}(R)$ after spacial averaging, given the previous approximation.

If we look at a system composed of some quantity ρ which decreases with time at a rate $\omega(t)$, the system is described by

$$\frac{d\rho}{dt} = -\omega(t)\rho$$

if $\omega(t)$ can be written as $\frac{df(t)}{dt}$

$$\frac{d\rho}{\rho} = - df(t)$$

and integrating

$$\rho = ce^{-f(t)} .$$

In a like manner $<\omega>$ might be written as

$$<\omega> = (c/c_o)\gamma^{-3} \frac{d}{dt} g(z),$$

Another possible approach to approximate $<\omega>$ is to consider the quantity appearing in the exponent of

$$e^{-[\beta_s^o t + \gamma^{-3}(c/c_o)g(z)]}.$$

The time dependence of the second term is contained in the complicated behavior of $g(z)$, yet it may be possible to approximate the second term as

$$<<\omega t> = \gamma^{-3}(c/c_o)g(z)$$

then

$$<\omega> = \gamma^{-3}(c/c_o)g(z)/t.$$

It will be shown that the latter is a better choice for $<\omega>$.

An important measurable quantity in time resolved spectroscopy is the ratio of the integrated activator intensity to the integrated

sensitizer intensity, I_a/I_s. From (4) and (7)

$$\frac{I_a}{I_s} = \frac{\beta_a^i m(t)}{\beta_s^i n(t)} = \frac{\beta_a^i m(o)}{\beta_s^i n(o)} e^{G-(\beta_a^o-\beta_s^o)t} + \frac{(\beta_a^i/\beta_s^i)\langle\omega\rangle}{\langle\omega\rangle - (\beta_a^o-\beta_s^o)} \left(e^{G-(\beta_a^o-\beta_s^o)t} - 1 \right) \quad (8)$$

where the superscripts i and o refer to intrinsic rates and intrinsic plus quenching rates respectively and the definition has been made

$$G = (c/c_o)\gamma^{-3} g(z)$$

$$G' = \frac{dG}{dt}.$$

Clearly $\langle\omega\rangle$ should be a monotonic decreasing function of time. As Figure 10 shows both the B/t and G′ satisfy this condition. Both log plots of G′ and G/t are nearly linear in the range of 1μs-10^3μs and have nearly equal slopes. It is then possible to write

$$G/t = At^{\rho}$$

$$G = Bt^{\rho}$$

and from an estimate of numbers made from Figure 10

$$G' \approx \frac{1}{5} G/t,$$

as a crude approximation.

Now replace $\langle\omega\rangle$ with G′ in Equation (8) and look at the behavior of the function I_a/I_s.

$$\frac{I_a}{I_s} = Ae^{G-bt} + \frac{BG}{G/5 - bt} (e^{G-bt}-1)$$

For sufficiently small t, $G>bt$ and the second term is positive. At $G/5 = bt$, I_a/I_s has a singularity and the second term remains

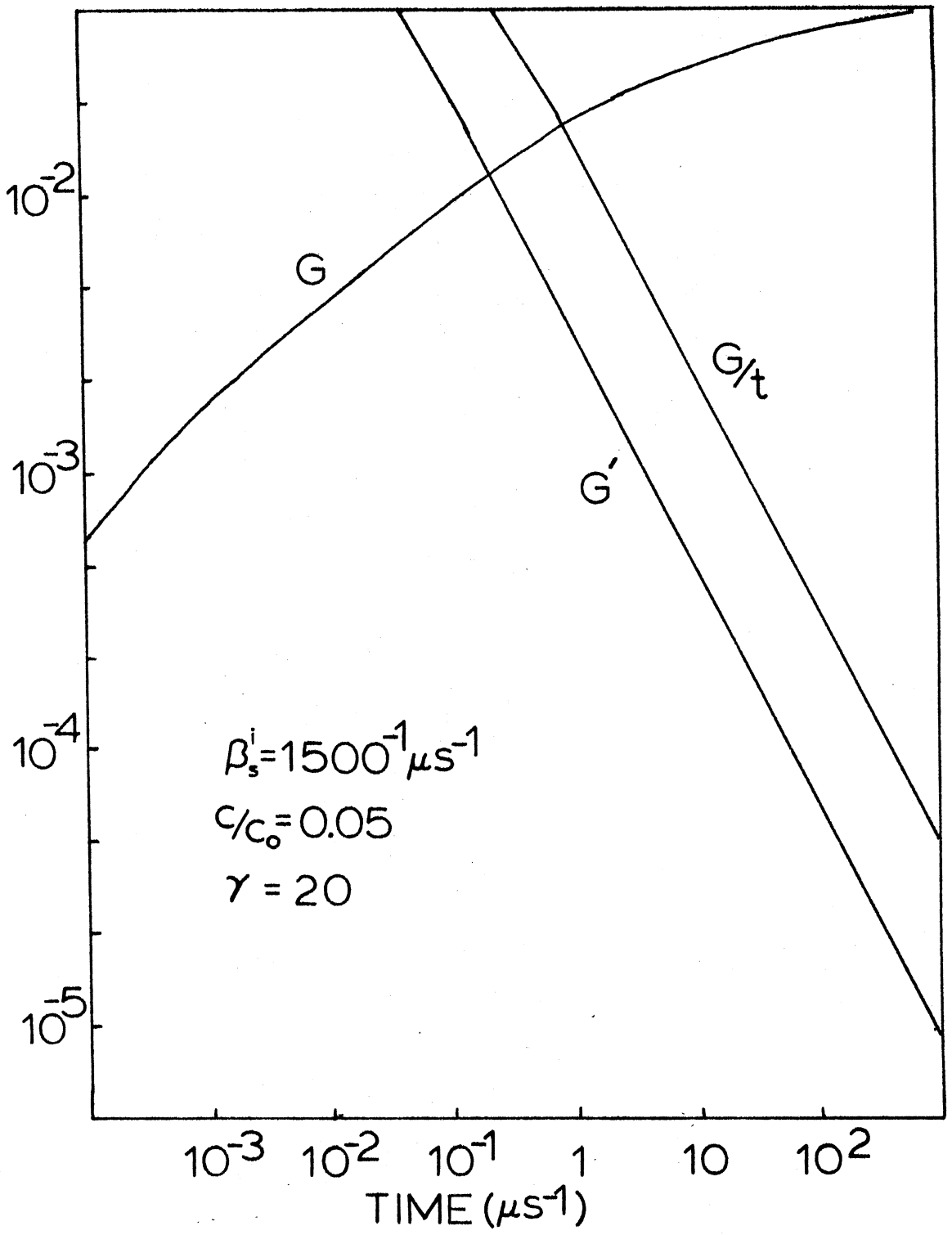

Figure 10. Functions G, G´, and G/t

negative for 5bt>G>bt. The net result is a behavior illustrated in Figure 11 for the milder cases of $G' = \frac{G}{1.1t}$ and $G' = \frac{G}{1.5t}$. $G' = \frac{G}{t}$ corresponds to the choice of $\langle\omega\rangle = \frac{G}{t}$. Then

$$\frac{I_a}{I_s} = Ae^{G-bt} + \frac{BG}{G-bt}\,(e^{G-bt}-1)$$

and in the limit $G \to bt$ the second term becomes GB (see Figure 11).

The important point to this analysis is that for a given parameter set, the function I_a/I_s, and hence the fit to the data, is relatively insensitive to the choice of $\langle\omega\rangle$ except for the distortion due to the singularity. Of course the distortion may be so bad as to make a fit impossible. Any singularity is obviously a symptom of the mathematical approximations made since no such behavior is physical; therefore, it seems reasonable to take $\langle\omega\rangle = G/t$ to obtain good fits without any pathological behavior. Finally,

$$\frac{I_a}{I_s} = \frac{\beta_a^i m(o)}{\beta_s^i n(o)}\, e^{G-(\beta_a^o-\beta_s^o)t} + \frac{\beta_a^i/\beta_s^i}{1-\frac{(\beta_a^o-\beta_s^o)t}{G}}\left(e^{G-(\beta_a^o-\beta_s^o)t} - 1\right). \qquad (9)$$

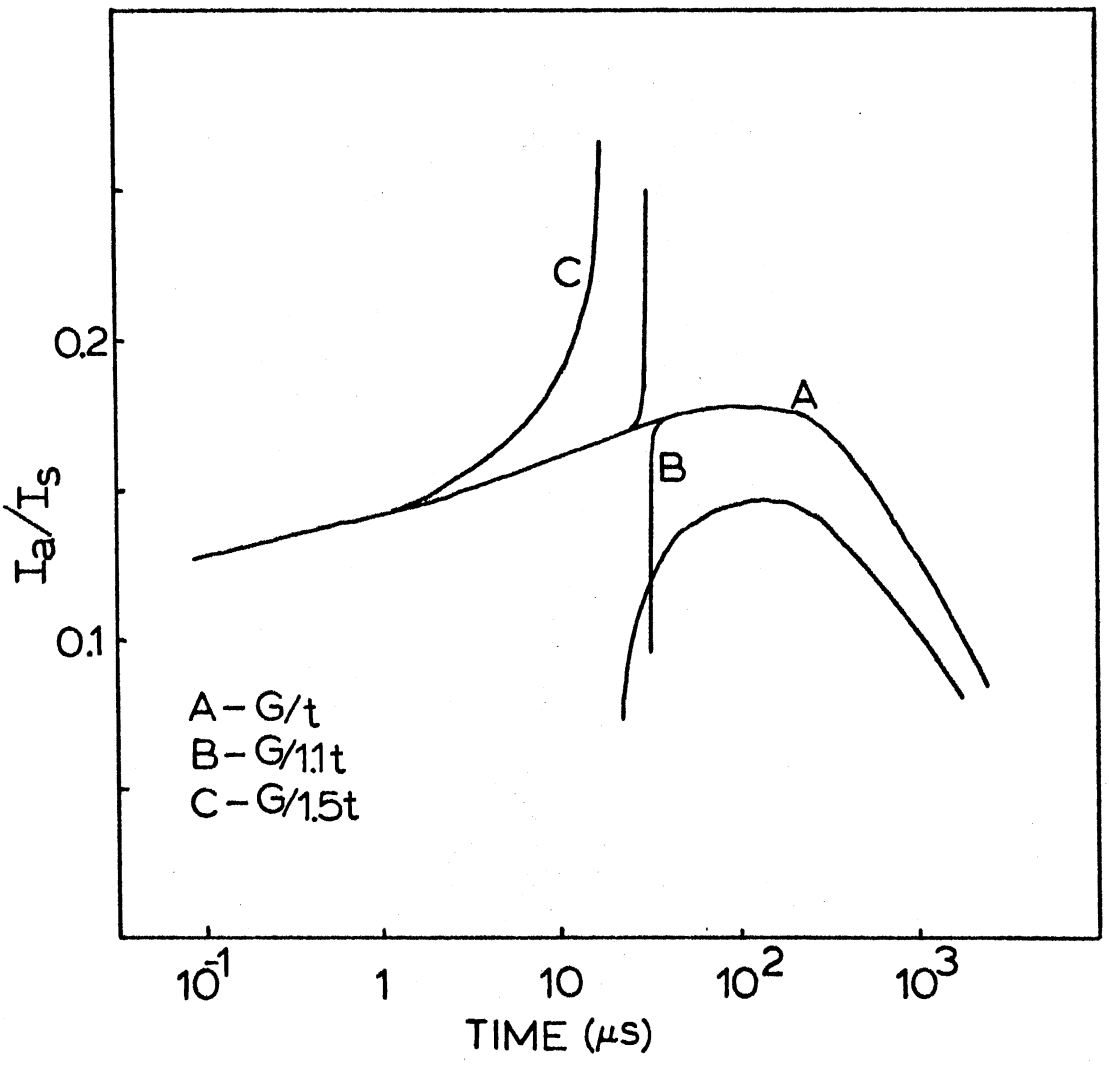

Figure 11. Representative Plot of I_a/I_s vs t for Parameters $c/c_o = .05$, $\gamma = 20$, $\beta_s^i = 1900^{-1}\mu s^{-1}$, $\beta_a^i = 740^{-1}\mu s^{-1}$, $\frac{m(o)}{n(o)} = .05$

CHAPTER III

EXPERIMENTAL RESULTS

Equipment Parameters

Listed here are a number of equipment conditions and parameters that are common to all of this chapter on Experimental Results.

The dye laser was charged with diphenylstilbene dissolved in p-dioxane. The laser was tuned to the narrow 4020 Å exitation peak by observing a maximum in the 5615 Å emission of the sensitizers, which the 4020 Å transition selectively excites. The peak in the exitation using this method was found to be 4019.9 $\pm$ 0.3 Å. It was possible to keep the linewidth of the dye laser less than 0.6 Å and usually in the range 0.4 - 0.5 Å.

The resolution of the spectrometer was always kept at 0.6 Å and calibration of the spectrometer was obtained by use of the 4415.7 Å emission line from a helium-cadmium laser.

Lifetimes of Sm^{3+} Ions in $CaWO_4$

Lifetimes at Low Temperature

At a temperature of $10^{o}K$ the two crystal field sites corresponding to 5615 Å emission (sensitizer) and 5632 Å emission (activator) have measurably different lifetimes as shown in Figure 12. At a concentration of 0.1% samarium and below, both sensitizer and activator

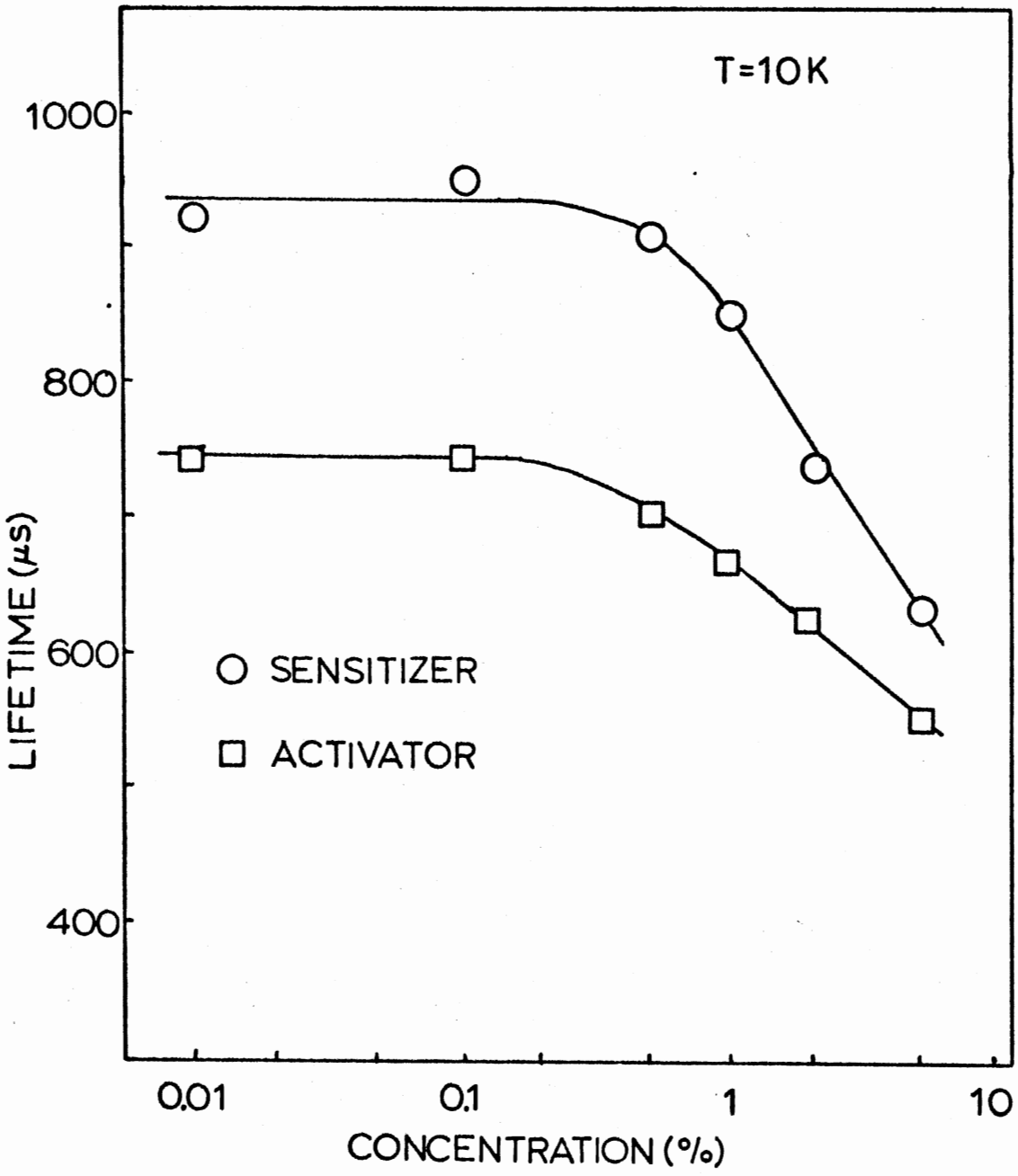

Figure 12. Lifetimes of Sensitizer and Activator Sites at Low Temperature

approach constant lifetimes of 940 μs and 740 μs respectively. The interpretation of this behavior is that at 0.5% concentration and greater concentration quenching processes and/or energy transfer becomes significant.

If the model of a two level system developed in Chapter II is assumed, the measured decay rates can be expressed as follows:

$$\beta_s = \beta_s^i + \beta_{qs} + \omega_{sa} \tag{10}$$

$$\beta_a = \beta_a^i + \beta_{qa} \ . \tag{11}$$

From (11)

$$\beta_a^i = \beta_a - \beta_{qa}$$

and at concentrations below 0.5% it is assumed $\beta_{qa} = 0$, therefore,

$$\beta_a^i = \beta_a(.1\%) = 1.35 \times 10^{-3} \mu s^{-1} \ .$$

If it is further assumed that the quenching processes and therefore the quenching rate is the same for sensitizers and activators:

$$\beta_{qa} = \beta_{qs} = \beta_q \ .$$

Having determined β_a^i, β_q can be determined for each concentration.

Then from (10)

$$\beta_s^i + \omega_{sa} = \beta_s - \beta_q$$

and values of $\beta_s^i + \omega_{sa}$ as a function of concentration can be determined as shown in Table I.

TABLE I

MEASURED DECAY RATES AND QUENCHING RATES FOR SENSITIZER AND ACTIVATOR SITES AT LOW TEMPERATURE

Concentration	β_a (μs^{-1})	β_a (μs^{-1})	β_a (μs^{-1})	$\beta_s^i + \omega_{sa}$ (μs^{-1})
0.01%	1.35×10^{-3}	1.09×10^{-3}	0	1.09×10^{-3}
0.1%	1.34×10^{-3}	1.04×10^{-3}	0	1.04×10^{-3}
0.5%	1.43×10^{-3}	1.11×10^{-3}	$.09 \times 10^{-3}$	1.02×10^{-3}
1.0%	1.52×10^{-3}	1.17×10^{-3}	$.17 \times 10^{-3}$	1.00×10^{-3}
2.0%	1.60×10^{-3}	1.36×10^{-3}	$.25 \times 10^{-3}$	1.11×10^{-3}
5.0%	1.81×10^{-3}	1.59×10^{-3}	$.46 \times 10^{-3}$	1.13×10^{-3}

Average $\beta_s^i + \omega_{sa} = 1.07 \times 10^{-3} \mu s^{-1}$

From Table I it is clear that $\beta_s^i + \omega_{sa}$ is independent of concentration of Sm^{3+}. Since β_s^i may be expected to be constant ω_{sa} is also a constant and may or may not be zero. An estimate of β_s^i is given in the next section and a discussion of the time averaged transfer rate will be taken up there.

Concentration Quenching

A quenching mechanism of the dipole-dipole type would give rise to a distance dependence of the quenching rate:

$$\beta_q \alpha \frac{1}{R^6}$$

$$\beta_q \alpha \left(\frac{1}{R^3}\right)^2$$

$$\beta_q \alpha C^2$$

where C is concentration.

The quenching rate versus concentration when fitted to a power law gives $\beta_q \alpha C^{-0.7}$. Clearly the quenching mechanism is not dipole-dipole strength. The best fit is obtained for a mechansim of exchange strength. Then

$$\beta_q \alpha e^{-R}$$

$$\beta_q \alpha e^{-(R^3)^{1/3}}$$

$$\beta_q \alpha e^{-C^{-1/3}}.$$

A plot of $\ell n \beta_q$ versus $C^{-1/3}$ is shown in Figure 13. Also shown is the average $Sm^{3+} - Sm^{3+}$ distance, R, based on a uniform distribution within

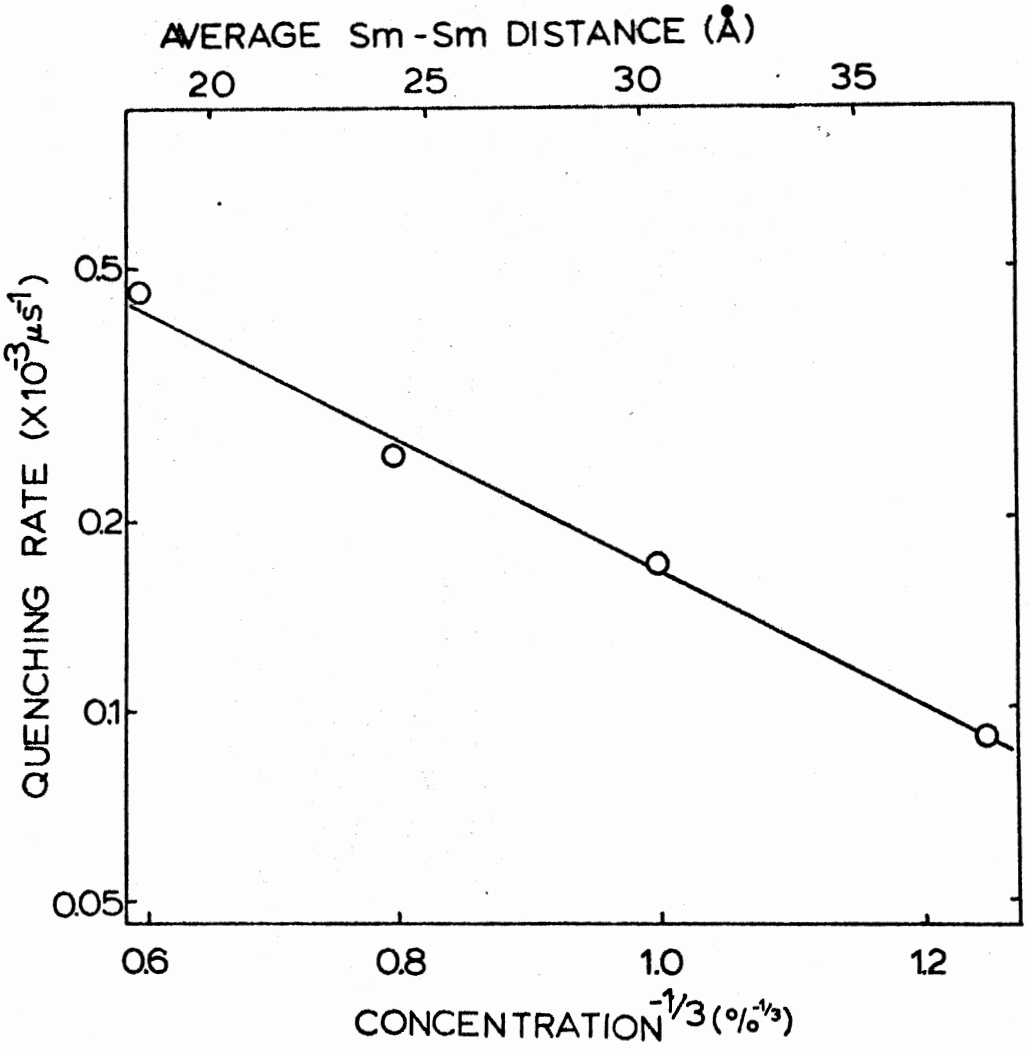

Figure 13. Quenching Rate in $CaWO_4:Sm^{3+}$

the crystal. Obtaining an estimate of L, the average Bohr radius for sensitizer and activator ions, from the slope of $\ell n \beta_q$ versus R gives a value of about 20 Å. L is expected to be on the order of 1 Å. Clearly the Sm^{3+} ions are not randomly distributed. If instead, L is taken to be 1 Å, an estimate can be made for ΔR, the variation in R necessary to produce the observed slope. Estimates show $\Delta R = 0.8$ Å. For comparison the nearest neighbor distance for Ca sites, into which the samarium substitutes, is 3.9 Å. The next nearest neighbor sites lie at distances of 5.2 Å and 6.5 Å.

It is possible that the narrow laser line (0.5 Å FWHM) used in this study selectively excites samarium ions in small clusters so that the samarium distribution is far from uniform, locally. Due to the limited range of the exchange interaction, exchange quenching is expected to occur only within a sphere of nearest neighbors. Also, because of the strong distance dependence, the interaction will occur predominently with the closest of the nearest neighbors. As an illustration, consider the following model.

Assume an exchange quenching that occurs only with the 16 nearest neighbor sites - 4 sites at 3.9 Å, 4 sites at 5.2 Å and 8 sites at 6.5 Å. Assume as well that quenching will occur only with the closest of the occupied sites. If one quenching center is placed in the 16 available sites, its average distance will be about 5.5 Å. As more quenching centers are added the average of the closest site will approach 3.9 Å, and is 4 Å for only 8 quenching centers. The difference in the average of the closest site over many configurations is in this case $\Delta R = 1.5$ Å.

The illustration may provide a hint as to the nature of the actual situation but no effort is made here to discuss the specifics. A proper treatment must take into account the fact that the probability for quenching is not one for the nearest of the quenching centers but is given by a probability which is proportional to e^{-R}, applied to all nearby quenching centers. In addition there is no reason to assume the mean number of quenching centers within a sphere of nearest neighbors is directly proportional to the concentration of samarium. It may be that for an exchange interaction, operating over small distances where the discrete nature of the lattice is important, a discrete or noncontinuum model for energy transfer would describe things better. Attempts have been made to do this (28) but no more will be done here than to mention it.

The nature of the quenching is suggested by VanUitert (3)(4) where he attributes concentration dependent quenching in tungstate host materials as being due to cross relaxation between a samarium in the ground state and a samarium in the excited state. The possible modes of cross relaxation are shown in Figure 14. It is interesting that VanUitert, monitoring 6450 $\mathring{A}$ emission from $CaWO_4:Sm^{3+}$, saw the onset of quenching at concentrations of 5% samarium and above, using broad band uv exitation. This, he attributed to a multipolar interaction. A 5% samarium concentration corresponds to an average samarium-samarium distance of 18 $\mathring{A}$. In this study quenching was observed beginning at 0.5%, which corresponds to an average samarium separation of 39 $\mathring{A}$.

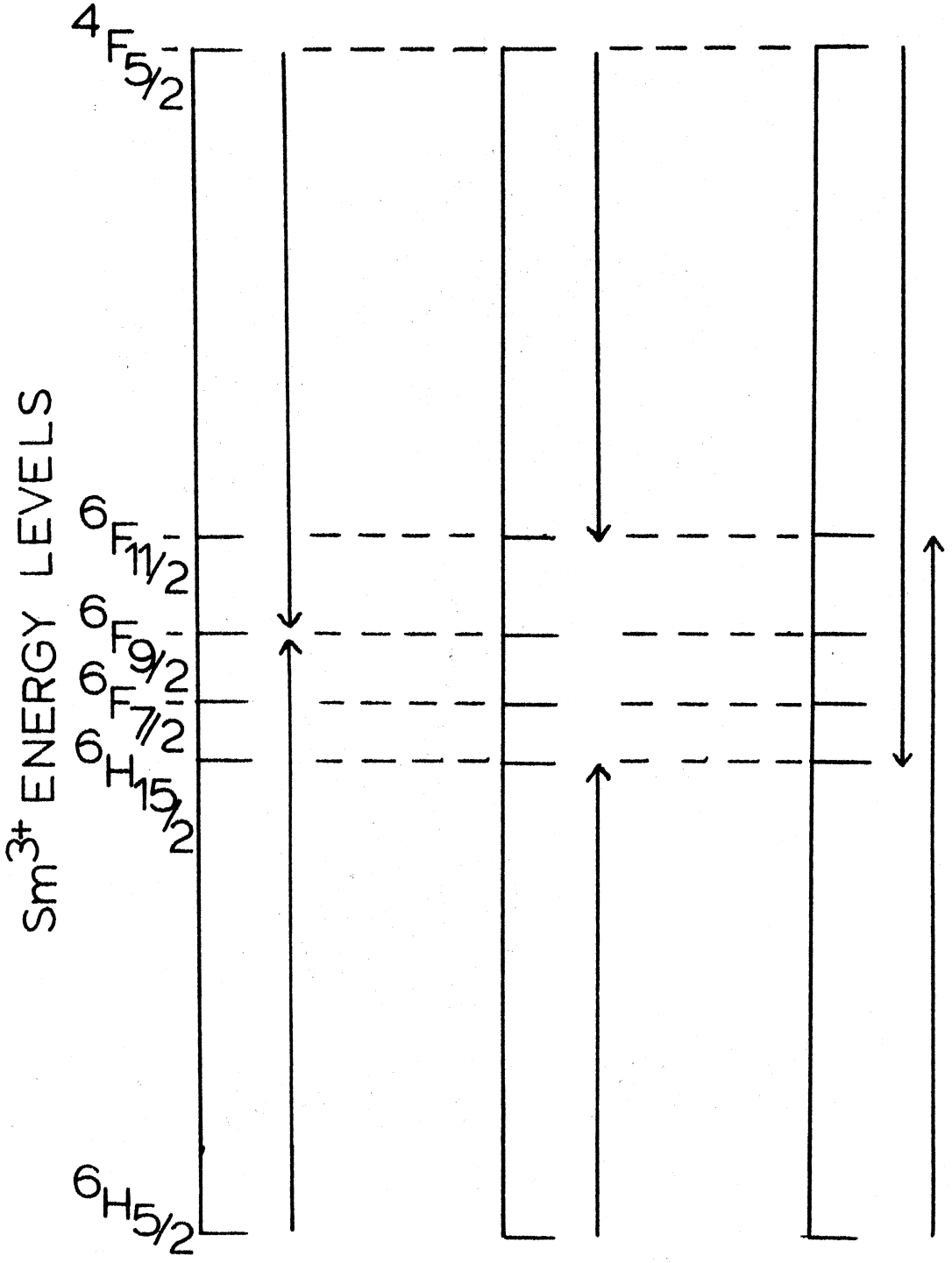

Figure 14. Cross Relaxation Schemes for Quenching in $CaWO_4:Sm^{3+}$

Lifetimes at High Temperature

A full temperature dependence of lifetimes was not done. Lifetimes were obtained for the sensitizer and activator at 130°K for the 5% sample and at 200°K for the 2% and 0.5% sample. The sensitizer lifetimes were unchanged. The activator lifetimes at high temperature approximated the sensitizer lifetimes as shown in Figure 15.

Energy Transfer at Low Temperature

Spectrum of sensitizer and activator lines were obtained as a function of time at a constant temperature of 10°K. The exitation wavelength of the laser source was 4020 Å as mentioned previously. The integrated intensity ratios were measured and plotted as a function of time as shown in Figures 16-19.

Exitation at 4020 Å is thought to selectively excite the sensitizer sites in the crystal which give rise to the fluorescence line at 5615 Å. Activator fluorescence is observed shifted to lower energy by 54 cm^{-1} and appears at 5632 Å.

Due to the energy mismatch and low temperatures involved it is reasonable to assume that energy transfer from activator to sensitizer (back transfer) will not be significant due to the scarcity of phonons at 10°K.

Determination of the type of interaction involved was based on the fits to the data at low temperature, so a discussion of the fitting is in order.

The sharp downturn seen in all the plots at about 200 μs precludes any fit where the transfer rate is considered constant, even if back

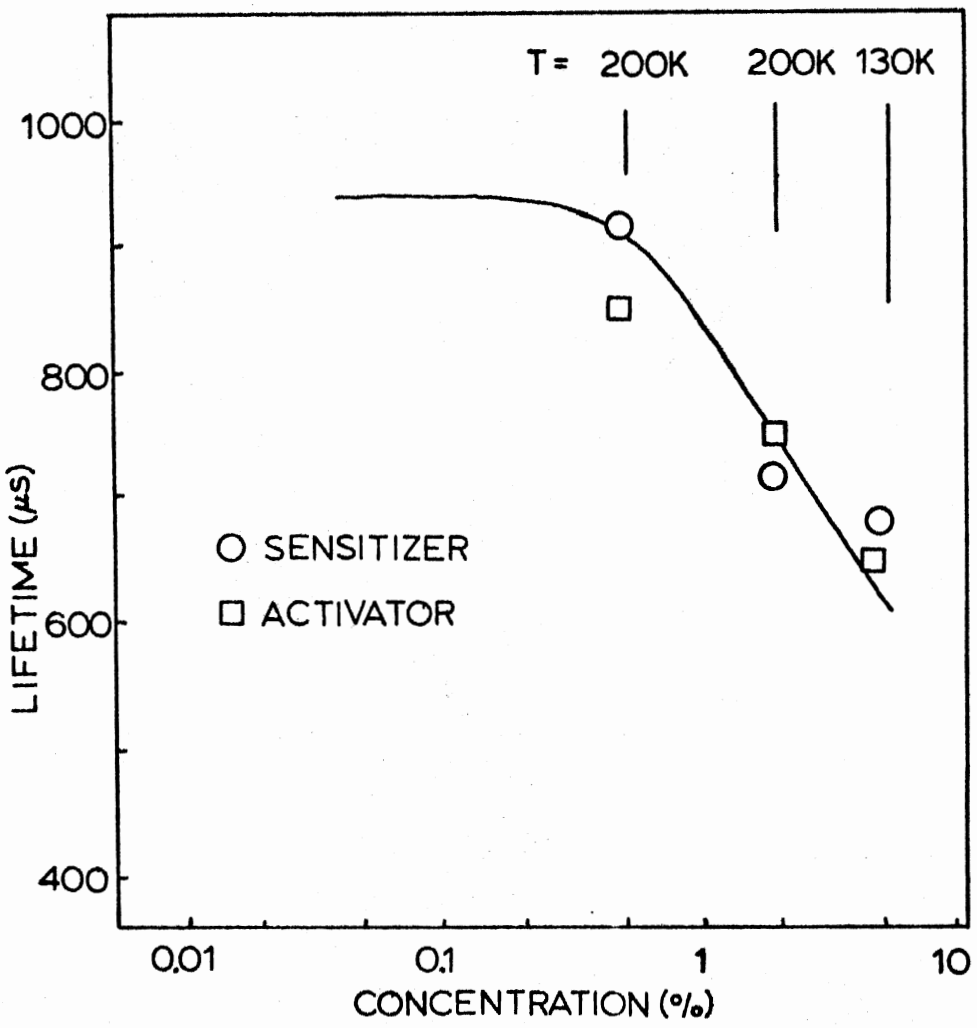

Figure 15. Lifetimes of Sensitizer and Activator Sites at High Temperature

TABLE II

LIFETIMES OF SENSITIZER AND ACTIVATOR SITES
AT HIGH TEMPERATURE

Concentration	Temperature (^{o}K)	τ_s (μs)	τ_a (μs)
0.5%	200	916	842
2.0%	200	711	744
5.0%	130	671	650

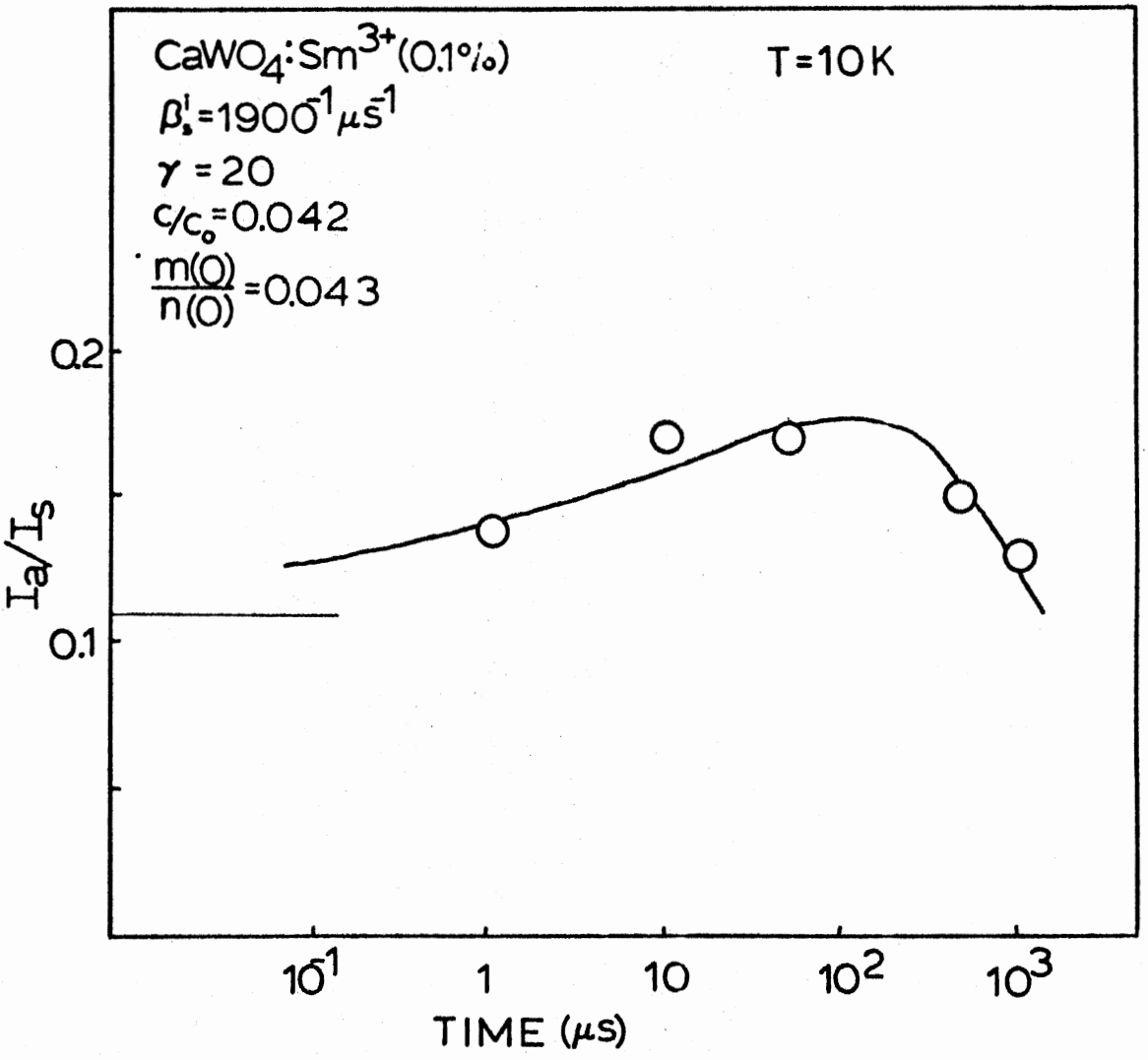

Figure 16. Energy Transfer at Low Temperature: 0.1% Sample

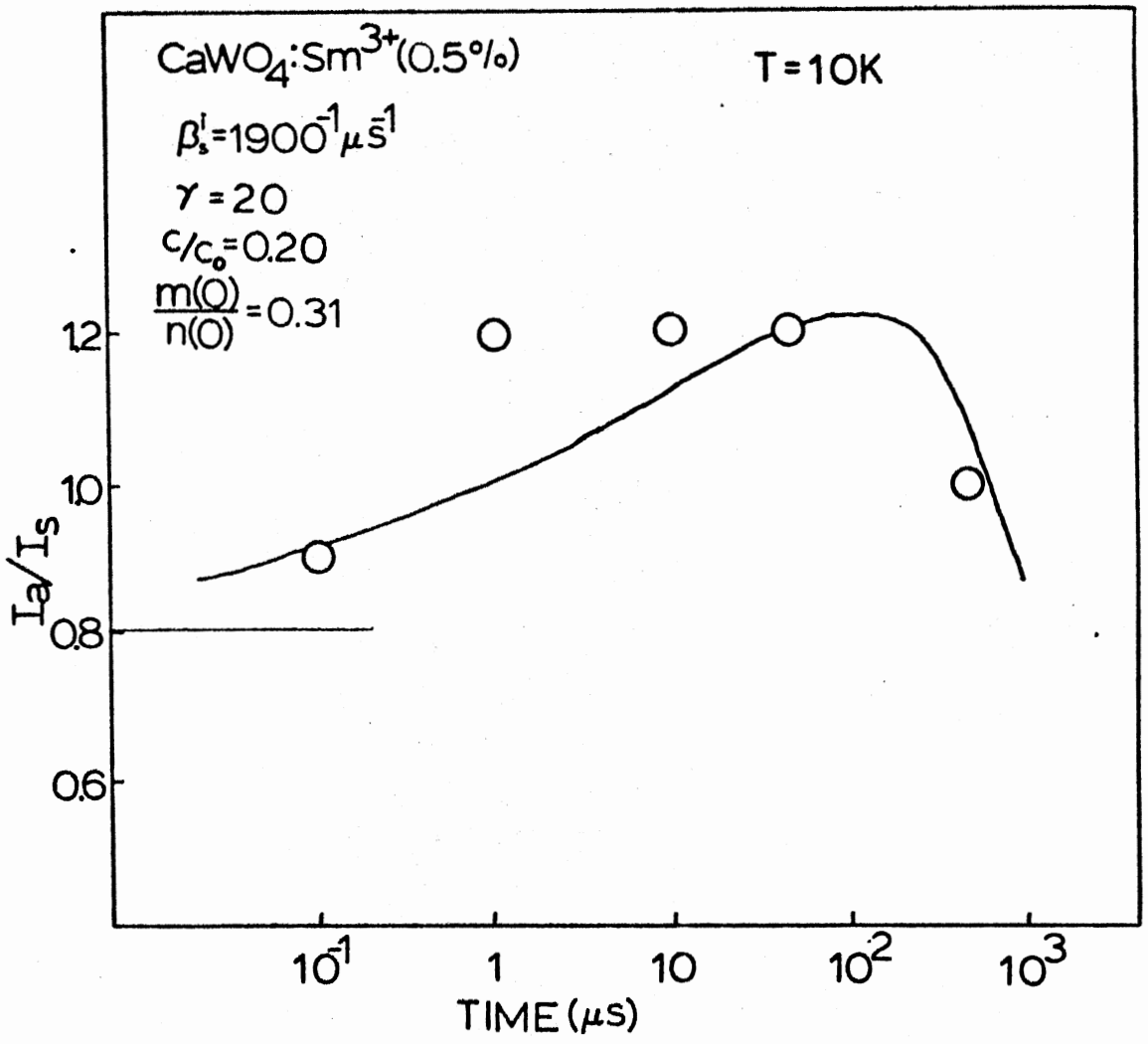

Figure 17. Energy Transfer at Low Temperature: 0.5% Sample

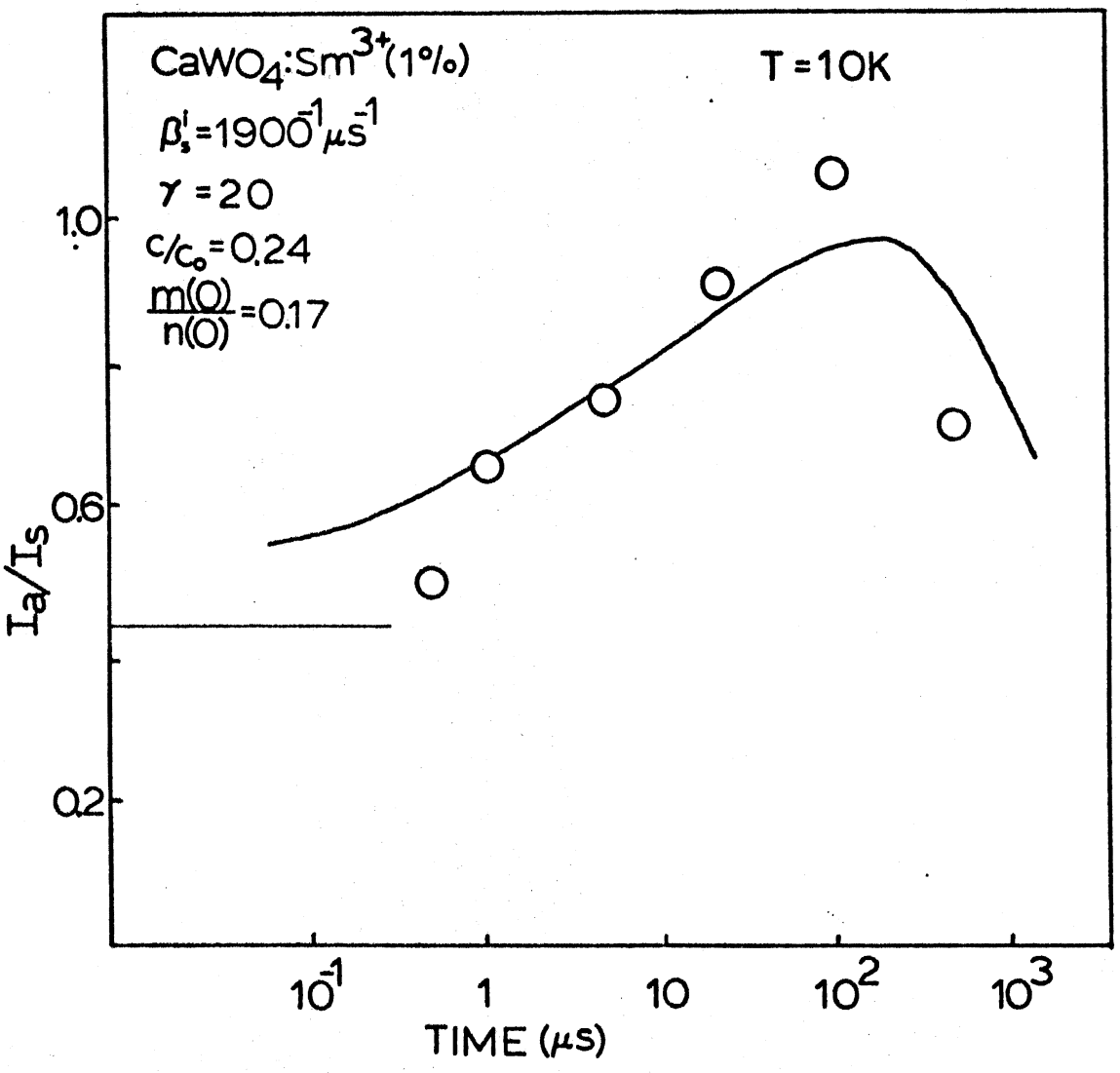

Figure 13. Energy Transfer at Low Temperature: 1% Sample

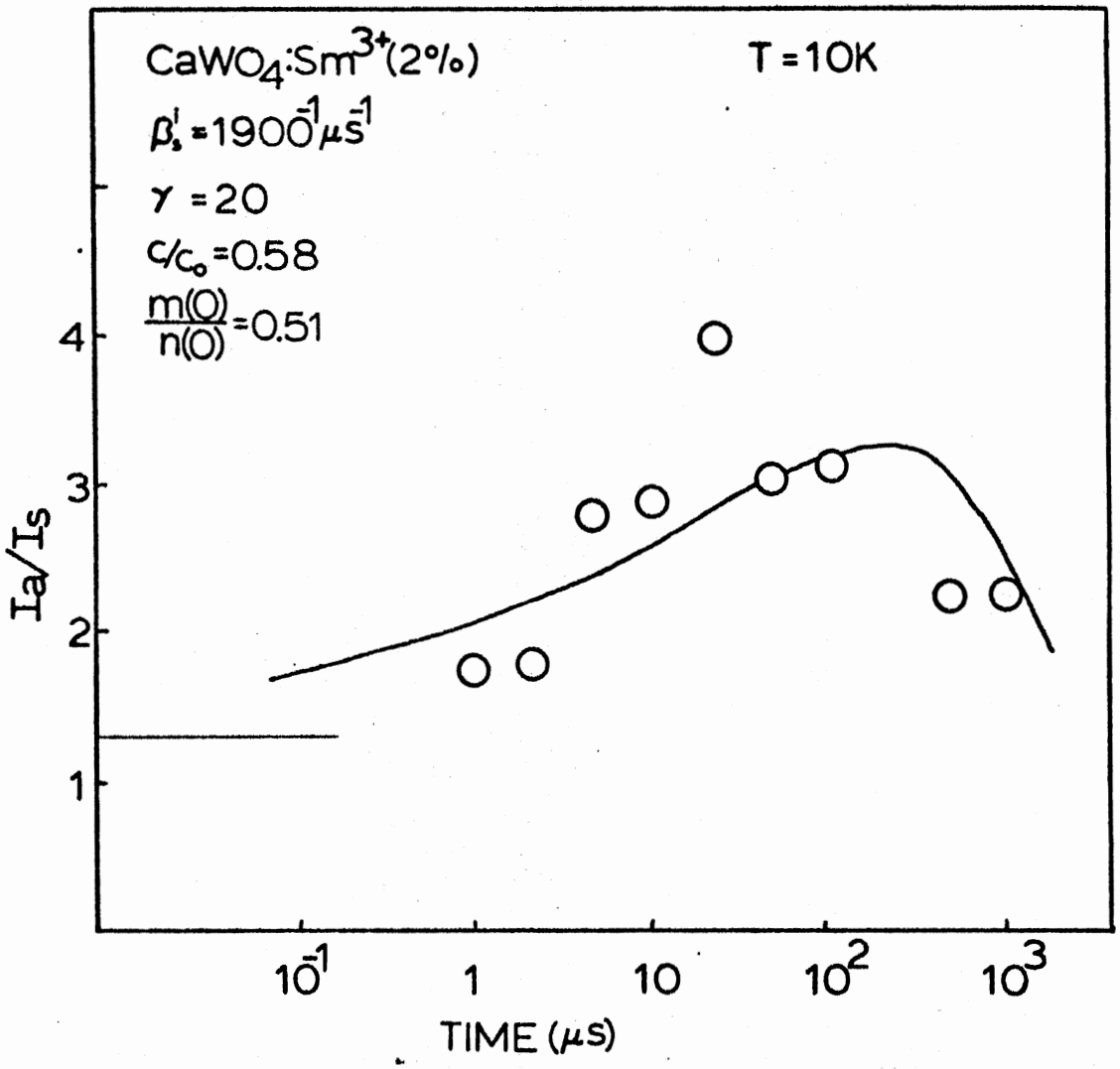

Figure 19. Energy Transfer at Low Temperature: 2% Sample

transfer is included. A time dependent rate is required to produce this behavior. Multipole interaction will produce a downturn but not the abrupt one seen here. The only interaction mechanism that could be made to fit the data was a time dependent transfer rate due to an exchange interaction. Fits are therefore based on the model for low temperature energy transfer discussed in Chapter II. From Equation (9)

$$\frac{I_a}{I_s} = \frac{\beta_a^i m(o)}{\beta_s^i n(o)} e^{c/c_o\gamma^{-3}g(z) - (\beta_a^o\beta_s^o)t}$$

$$+ \frac{\beta_a^i/\beta_s^i}{1 - \frac{(\beta_a^o-\beta_s^o)t}{c/c_o\gamma^{-3}g(z)}} \left(e^{c/c_o\gamma^{-3}g(z) - (\beta_a^o-\beta_s^o)t} - 1 \right)$$

where as before the superscript i refers to intrinsic lifetime and the superscript o refers to the intrinsic rate plus the quenching rate.

The decay rate β_s^o is not known, since the intrinsic rate β_s^i is not known. β_s^o is then rewritten as $\beta_s^o = \beta_s^i + \beta_q$, and

$$\frac{I_a}{I_s} = \frac{\beta_a^i m(o)}{\beta_s^i n(o)} e^{c/c_o\gamma^{-3}g(z) - (\beta_a^o-\beta_s^i-\beta_q)t}$$

$$+ \frac{\beta_a^i/\beta_s^i}{1 - \frac{(\beta_a^o-\beta_s^i-\beta_q)t}{c/c_o\gamma^{-3}g(z)}} \left(e^{c/c_o\gamma^{-3}g(z) - (\beta_a^o-\beta_s^i-\beta_q)t} - 1 \right)$$

A fit is accomplished by variation of the parameters c/c_o, γ, and β_s^i. At t=o

$$\frac{I_a}{I_s} = \frac{\beta_a^i m(o)}{\beta_s^i n(o)}$$

so that $\frac{m(o)}{n(o)}$ is known for a given β_s^i.

In general a three parameter fit is a difficult problem, but in this case the effect of each of the three parameters is relatively independent. A vertical translation is the general effect of changing c/c_o, γ effects the steepness of the rise in I_a/I_s, and β_s^i determines the position of the peak of the curve. The parameters obtained are summarized in Table III.

Best fits are obtained for $\gamma = 20$ and $\beta_s^i = 1900^{-1}\mu s^{-1}$. From the development of the exchange interaction in Chapter II, and for $L \sim 1.0$ Å, a value $\gamma = 2R_o$ is obtained for R_o of about 10 Å. A theoretical estimate of R_o cannot be made without a knowledge of the wavefunction overlap but the obtained values are not unreasonable. From an analysis of lifetimes as a function of concentration in the previous section, it was determined $\beta_s^i + \langle\omega\rangle_t = 1.07 \times 10^{-3}\mu s^{-1}$. This yields an estimate for the time averaged transfer rate:

$$\langle\omega\rangle_t = .54 \times 10^{-3}\mu s^{-1}.$$

Energy Transfer at High Temperature

Introduction

At high temperatures (200^oK), the simple model illustrated in Figure 20 was found sufficient to account for the observed behavior of

TABLE III

FITTING PARAMETERS FOR LOW TEMPERATURE ENERGY TRANSFER

Concentration (o/o)	$\frac{m(o)}{n(o)}$	c/c_o
.1	.043	.042
.5	.31	.20
1.0	.17	.24
2.0	.51	.58

$\gamma = 20$

$\beta_s^i = 1900^{-1} \mu s^{-1}$

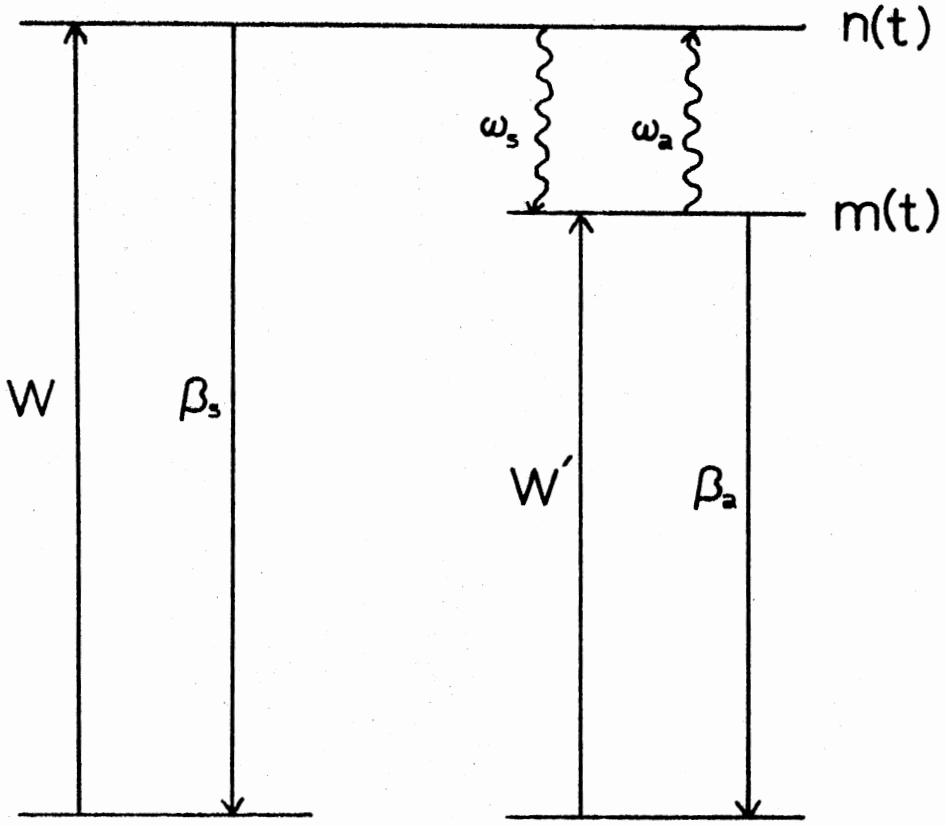

Figure 20. Model for Energy Transfer at High Temperature

TABLE IV

INTEGRATED INTENSITY RATIOS VS TIME AT $10^{o}K$

$CaWO_4:Sm^{3+}$									T = $10^{o}K$
				0.1%					
Time (μs)	1	10	50	500	1000				
I_a/I_s	.14	.17	.17	.15	.13				
				0.5%					
Time (μs)	.1	1	10	50	500				
I_a/I_s	.09	.12	.12	.12	.10				
				1.0%					
Time (μs)	.5	1	5	20	100	500			
I_a/I_s	.48	.65	.75	.90	1.03	.70			
				2.0%					
Time (μs)	1	2	5	10	20	50	100	500	1000
I_a/I_s	1.81	1.81	2.78	2.92	3.98	3.02	3.12	2.24	2.30

the ratio of the integrated intensities as a function of time. The forward sensitizer-activator transfer rate as well as the back transfew rate is considered a constant. A constant transfer rate implies transfer from sites with identical environments. If the transfer consists of many steps, then the average step can be characterized as a series of steps from the same type of sensitizer environment. Many steps therefore, has the effect of averaging out the time dependence of the transfer rate. The constant ratio at long times indicates the population of excited sensitizers and activators in thermal equilibrium.

The rate equations can be written down, describing the sensitizer and activator populations:

$$\frac{dn(t)}{dt} = W - (\beta_s + \omega_s)n(t) + \omega_a m(t) \tag{12}$$

$$\frac{dm(t)}{dt} = W' - (\beta_a + \omega_a)m(t) + \omega_s n(t) \tag{13}$$

If $\beta_a = \beta_s$ the solution is simplified considerably. This is probably a reasonable assumption since the sensitizer lifetime seems independent of temperature and the measured activator lifetime is the same as the sensitizer lifetime at 200°K. Equations (12) and (13) then give

$$n(t) = \frac{\omega_a(n(o) + m(o))}{\omega_s + \omega_a} e^{-\beta t} + \frac{\omega_s n(o) - \omega_a m(o)}{\omega_s + \omega_a} e^{-(\beta+\omega_s+\omega_a)t}$$

$$m(t) = \frac{\omega_s(n(o) + m(o))}{\omega_s + \omega_a} e^{-\beta t} + \frac{\omega_a m(o) - \omega_s n(o)}{\omega_s + \omega_a} e^{-(\beta+\omega_s+\omega_a)t}$$

Then

$$\frac{I_a}{I_s} = \frac{m(t)}{n(t)} = \frac{\frac{\omega_s}{\omega_a}\left(\frac{m(o)}{n(o)} + 1\right) - \left(\frac{\omega_s}{\omega_a} - \frac{m(o)}{n(o)}\right)e^{-(\omega_s+\omega_a)t}}{\left(\frac{m(o)}{n(o)} + 1\right) + \left(\frac{\omega_s}{\omega_a} - \frac{m(o)}{n(o)}\right)e^{-(\omega_s+\omega_a)t}} \tag{14}$$

Note that at $t = o$

$$\frac{I_a}{I_s} = \frac{m(o)}{n(o)}$$

and at long time, $t \to \infty$

$$\frac{I_a}{I_s} = \frac{\omega_s}{\omega_a} .$$

The data is fit using $\omega_s+\omega_a$ as an adjustable parameter. Results for the 2% sample are shown in Figure 21 and Table VI.

It should be noted here that Hsu and Powell obtained fits using the same model as is described here, though their numbers are different.

Temperature Dependence of the Transfer Rates

It was seen in the previous section that for sufficiently long times at high temperature,

$$\frac{I_a}{I_s} \approx \frac{\omega_s}{\omega_a} .$$

The constant transfer ratio at long time is interpreted as meaning the populations of excited sensitizers and activators are in thermal equilibrium.

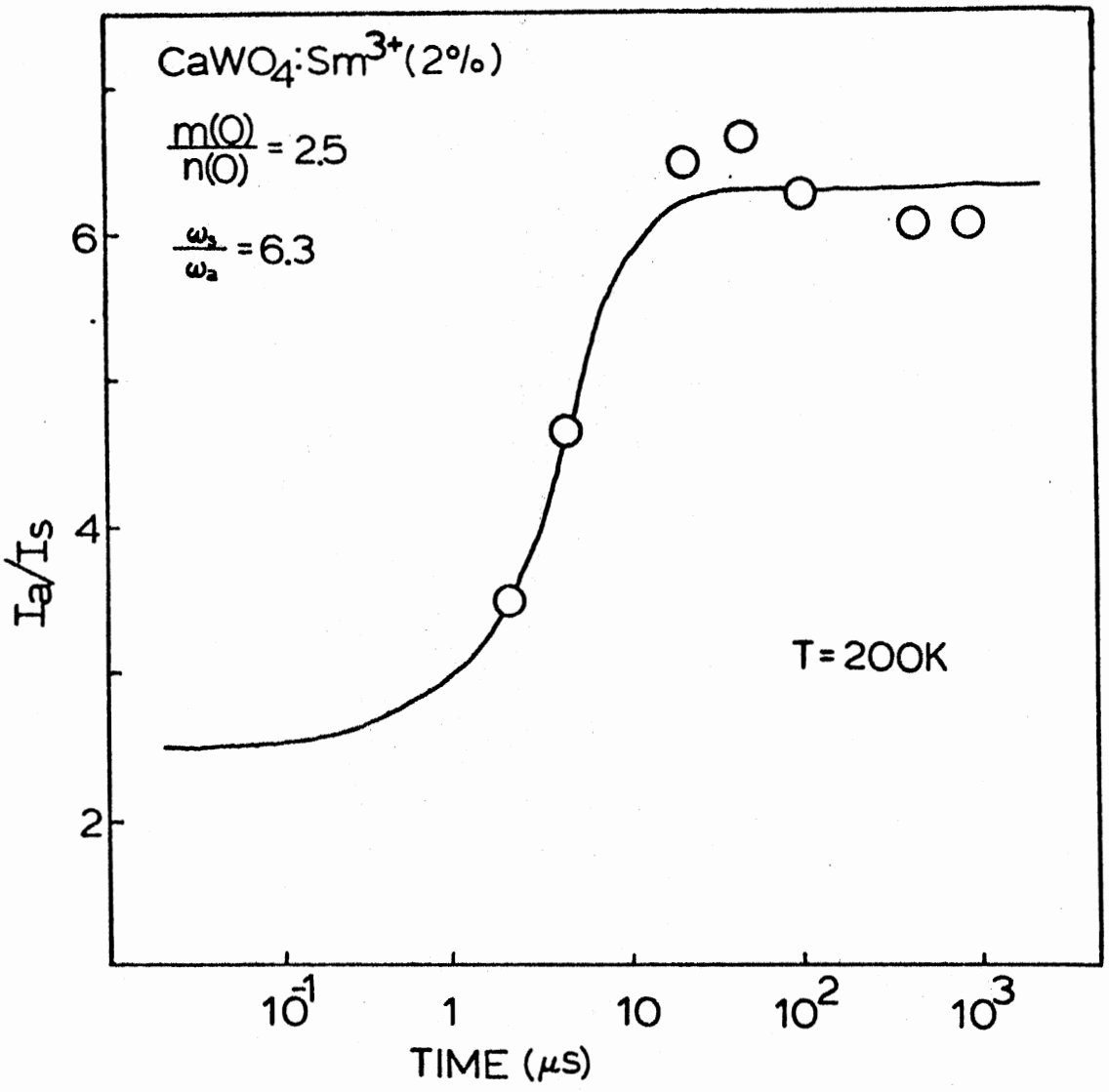

Figure 21. Energy Transfer at High Temperature: 2% Sample

TABLE V

INTEGRATED INTENSITY RATIO VS TIME AT 200°K

$CaWO_4:Sm^{3+}$ (2%)

T = 200°K

Time (μs)	I_a/I_s
2	3.5
5	4.7
20	6.5
50	6.7
100	6.3
200	6.1
500	6.1

TABLE VI

SUMMARY OF ENERGY TRANSFER PARAMETERS AT 200°K
FOR 2% SAMPLE

ω_s/ω_a	$\frac{m(o)}{n(o)}$	$(\omega_s+\omega_a)(\mu s^{-1})$	$\omega_s(\mu s^{-1})$	$\omega_a(\mu s^{-1})$
6.3	$2.5 \pm .3$	.27	$.23 \pm .05$	$.037 \pm .007$

For transfer to take place from sensitizer to activator, energy equal to the amount of the energy mismatch must be given up to the lattice. For the case when the energy mismatch, ΔE is about 54 cm^{-1}. The same energy must be supplied by the lattice for back transfer to occur. Holstein, Lyo, and Orback have derived an expression for the temperature dependence of the transfer rate for the simple case where ΔE is supplied by a single lattice phonon (29). The temperature dependence of the single phonon assisted transfer rate can be written

$$\omega_{12} \alpha \begin{cases} e^{\Delta E/kT} \Big/ (e^{\Delta E/kT} - 1) & \text{for phonon emission} \\ 1 \Big/ (e^{\Delta E/kT} - 1) & \text{for phonon absorption} \end{cases}$$

Then

$$\frac{I_a}{I_s} = \frac{\omega_{sa}}{\omega_{as}} = e^{\Delta E/kT} \tag{15}$$

The integrated intensity ratio as a function of temperature, measured for the 2% sample is shown in Figure 22. The behavior of I_a/I_s predicted by Equation (15) is opposite to that observed. As already mentioned, energy transfer at high temperature is best described by a multistep sensitizer-sensitizer migration terminated by a sensitizer-activator transfer. A proper description of the temperature dependence is given by

$$\frac{I_a}{I_s} \alpha \omega_{ss} \frac{\omega_{sa}}{\omega_{as}} \tag{16}$$

where ω_{ss} describes the migration of energy from sensitizer to

TABLE VII

TEMPERATURE DEPENDENCE OF THE INTEGRATED INTENSITY RATIO

2% Sample	
$T(^{o}K)$	I_a/I_s
10	2.2
30	1.7
50	2.0
80	3.2
120	4.8
200	6.1

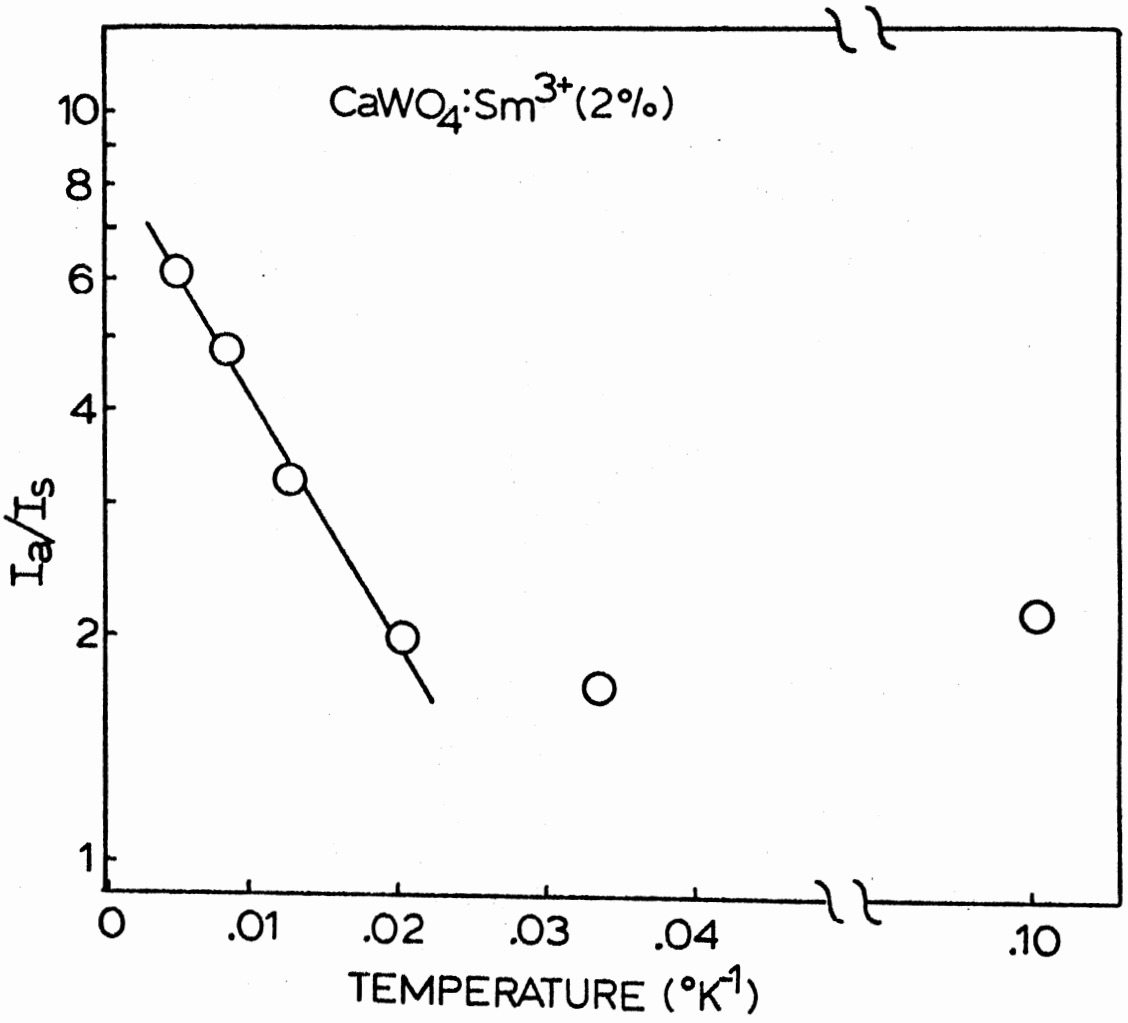

Figure 22. The Integrated Intensity Ratio as a Function of Temperature

sensitizer and ω_{sa} represents the last step in the chain - the transfer of energy from sensitizer to activator.

The data in Figure 22 is best fit by an exponential of the form

$$\frac{I_a}{I_s} \alpha e^{-E/kT} \quad \text{where } E \approx 52 \text{ cm}^{-1}. \tag{17}$$

Points below 50°K cannot be fit with the exponential used above, however the model being used is expected to break down at low temperatures where a single step time dependent rate is needed to describe the system.

The temperature dependence of ω_{ss} may be deduced by substituting (15) and (17) into (16)

$$\omega_{ss} \alpha e^{-(52 \text{ cm}^{-1} + \Delta E)/kT} \alpha e^{-\delta/kT} \tag{18}$$

where for $\Delta E = 54 \text{ cm}^{-1}$, $\delta = 106 \text{ cm}^{-1}$. The form of (18) suggests the existence of a new level shifted to higher energy by 106 cm^{-1} which, at high temperatures, becomes available to enhance energy migration among sensitizers. Reference to Figure 5 shows there is no 106 cm^{-1} splitting in the $^6H_{5/2}$ ground state, yet the possibility that an excited state splitting in the $^4F_{5/2}$ level cannot be overlooked. If there exists a 106 cm^{-1} splitting in the $^4F_{5/2}$ level, the three lines at 5632, 5654, and 5704 Å seen by Treadway and Powell at 8°K should be supplemented by three additional lines shifted by 106 cm^{-1} and appearing at 5600, 5621, and 5670 Å at room temperature. A steady state room temperature emission spectra taken by Treadaway (23) shows clearly two of these lines as shown in Figure 23. Indications

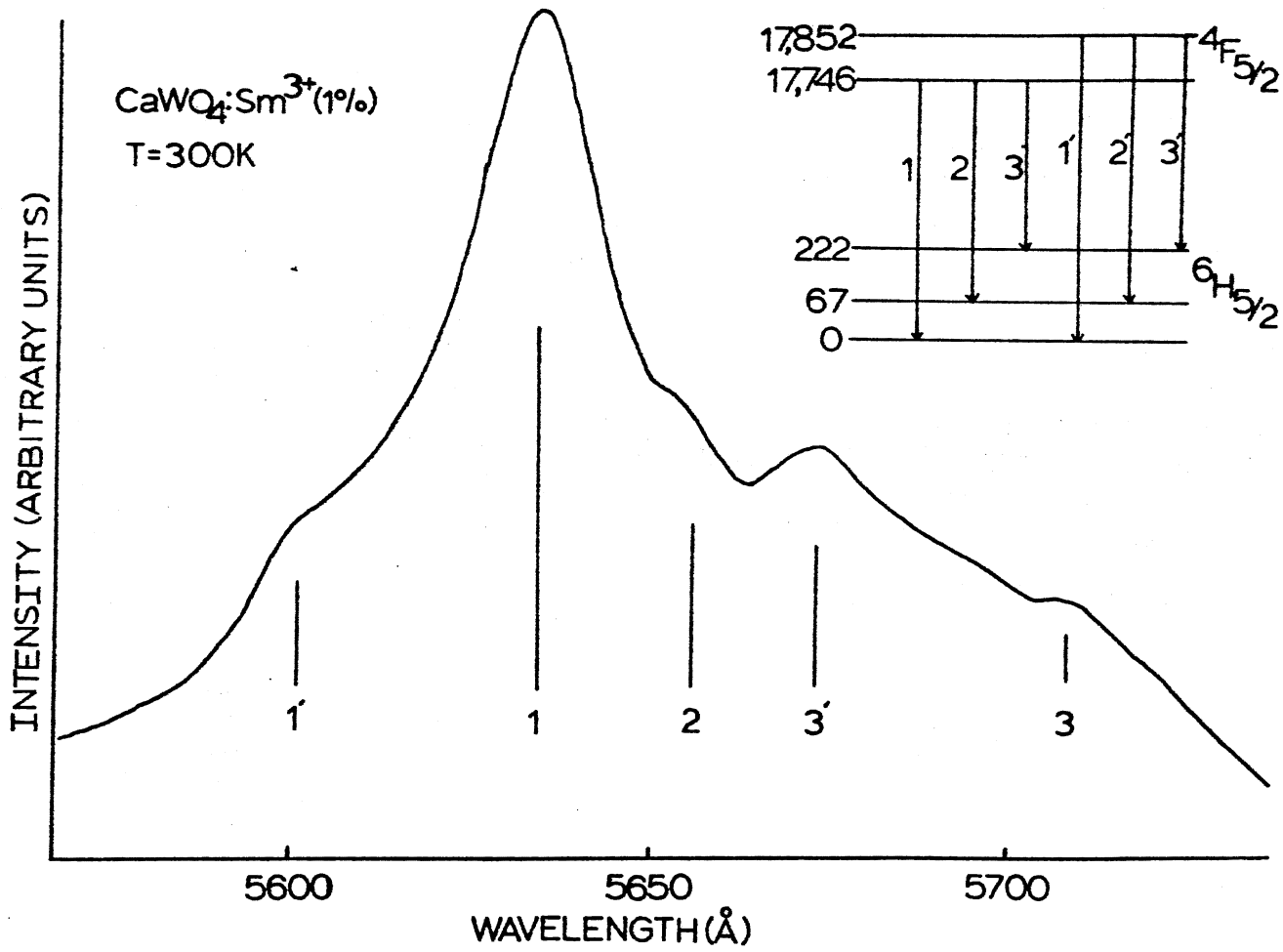

Figure 23. Steady State Fluorescence Spectra of $CaWO_4:Sm^{3+}$ at $300^{o}K$: 1% Sample

are that the $^4F_{5/2}$ level is split by 106 cm^{-1} and that the accessibility of this level at higher temperatures is responsible for the increased energy migration rate. Two possible mechanisms which could account for the temperature dependence of ω_{ss} are due to Weber (30) and Holstein, Lyo, and Orback (29).

Weber proposed that sensitizer-sensitizer energy migration could be enhanced if there occurred thermal population of a higher level resulting in a transition with a larger oscillator strength than that of the lower lying level. Since the energy transfer rate for a pair of ions is proportional to the oscillator strength, the energy transfer rate could increase dramatically.

The transition involved here is a $^4F_{5/2}$-$^6H_{5/2}$ transition and the 106 cm^{-1} splitting is within the $^4F_{5/2}$ manifold. The transitions are therefore forbidden ones and the oscillator strengths of transitions from the various Stark levels should be similar. The intensities observed in Figure 23 support this. The ratio of the integrated intensities of the 5632 line to the 5600 line and of the 5707 line to the 5670 line is clearly of order one. The Boltzman distribution correction to the intensity for 106 cm^{-1}, and a temperature of 300^oK is also of order one, so the oscillator strengths do not differ significantly.

Holstein, Lyo and Orback have shown that if another ionic level lies close to those participating in energy transfer, then a resonant phonon assisted process dominates. The temperature dependence becomes

$$\omega_{ss} \alpha e^{-\delta/kT}$$

where δ is the energy level splitting of the new participating level.

From (16), this gives

$$\frac{I_a}{I_s} = \frac{\omega_{ss}\omega_{sa}}{\omega_{as}} \alpha\ e^{-(\delta-\Delta E)/kT}$$

which gives the observed behavior.

Effect of Uniaxial Stress on Energy Transfer

A final experiment was performed to determine the effect of uniaxial stress on the ratio of the transfer rates and on fluorescence lifetimes. A similar experiment was done by Hsu and Powell on Sm^{3+} in $CaWO_4$, the difference being they were looking at a multistep diffusion process via the electric quadrupole-quadrupole interaction. The basic idea of the experiment can be explained with reference to Figure 24. Pressure is applied along the a_1 axis and light with a propagation direction along the c axis and polarization parallel to a_1 is incident on the crystal. Consider a Sm^{3+} ion substituting for the central ion site and a Na^+ or vacancy located at one of the sites displaced in the a_1 and c directions. The polarized incident light excites these dipoles. The pressure induced change in ionic separation of the Sm^{3+}-charge compensator pair is expected to perturb the level positions somewhat and this may result in a change in the observed transition energies. A Sm^{3+}-charge compensator pair with the charge compensator displaced in the a_2 and c directions will undergo no relative displacement and hence there will be no change in the observed transition energies.

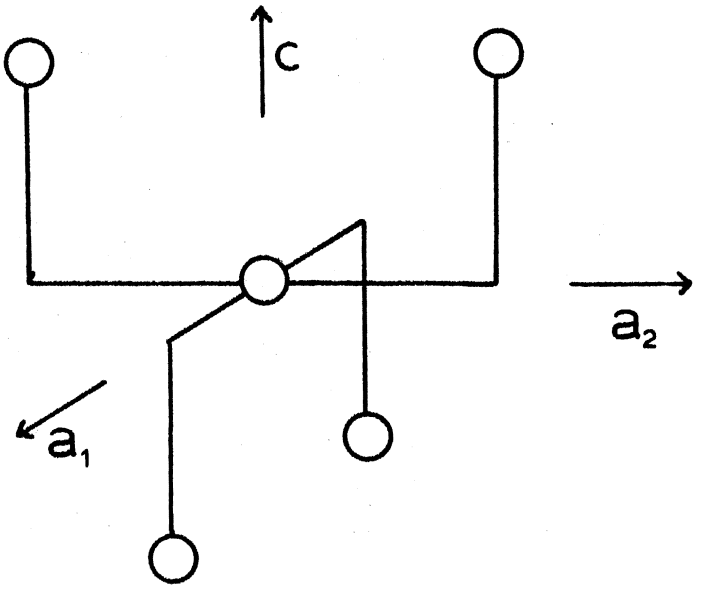

Figure 24. Configuration of Nearest Neighbor Cations in $CaWO_4$

Hsu and Powell observed a shifting of the sensitizer line to lower energies as well as inhibited energy migration due to the shifted pairs being out of resonance with the nonshifted pairs.

For this study there were no observable effects due to uniaxial stress. The position of the sensitizer emission line remained unchanged to within 0.2 $\mathring{A}$. The ratio of the transfer rates, as measured by the ratio of the integrated intensities, as well as the lifetimes showed no definite change. Figures 25-30 show these results.

It should be emphasized that the previous work alluded to and this work were substantially different. Hsu and Powell used an exitation laser source with a power output an order of magnitude less than the one used here. In addition they used a laser linewidth of 4 $\mathring{A}$ compared with the 0.5 used here. The interaction mechanisms under these conditions were an exchange interaction seen in this study compared with a quadrupole-quadrupole interaction seen by Hsu and Powell. The experiment is interesting in that it contrasts with results obtained under different conditions. In itself, however, the negative result obtained here proves nothing regarding the existence of any effect, except that the effect was not able to be detected.

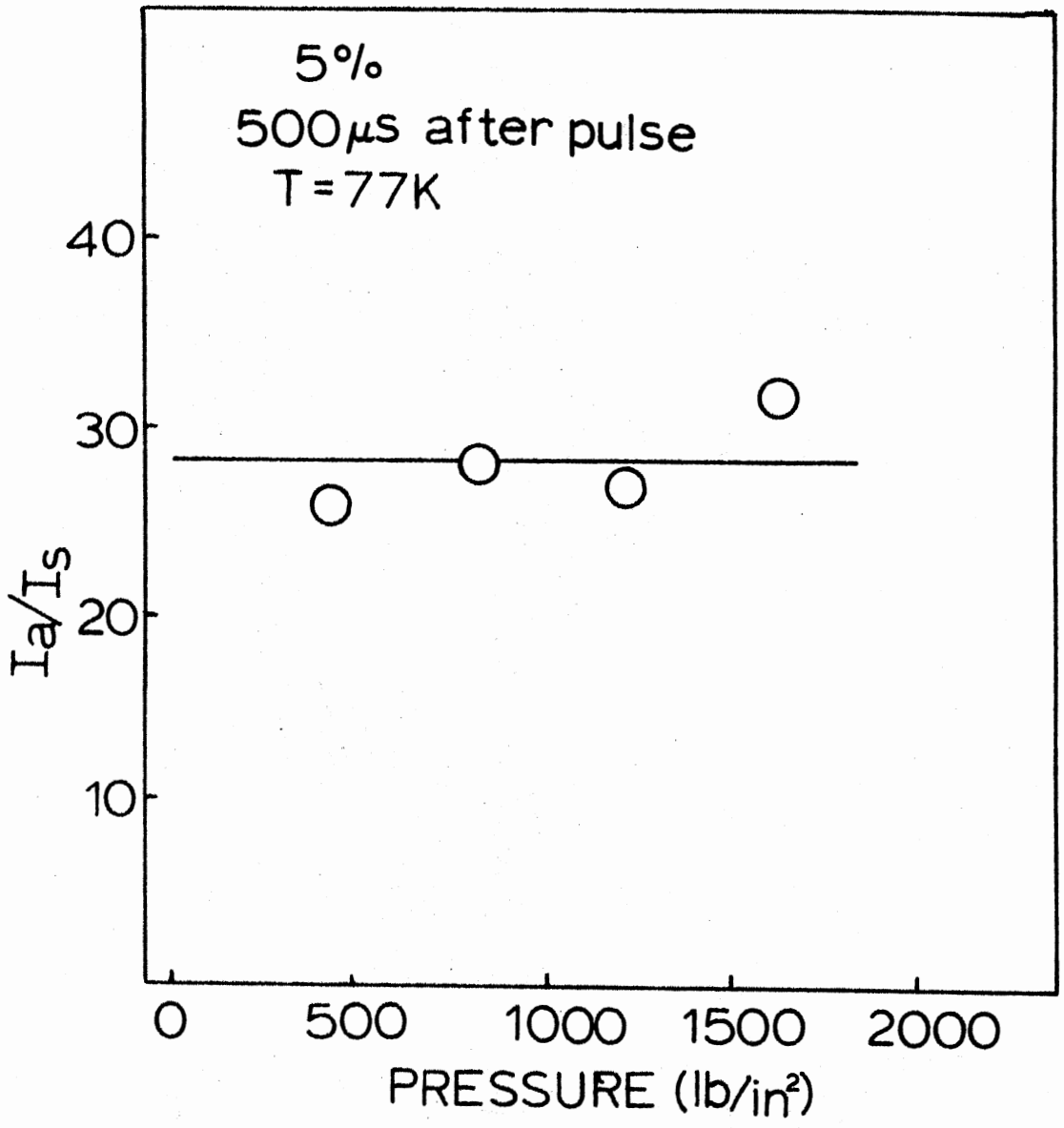

Figure 25. Effect of Uniaxial Stress on I_a/I_s

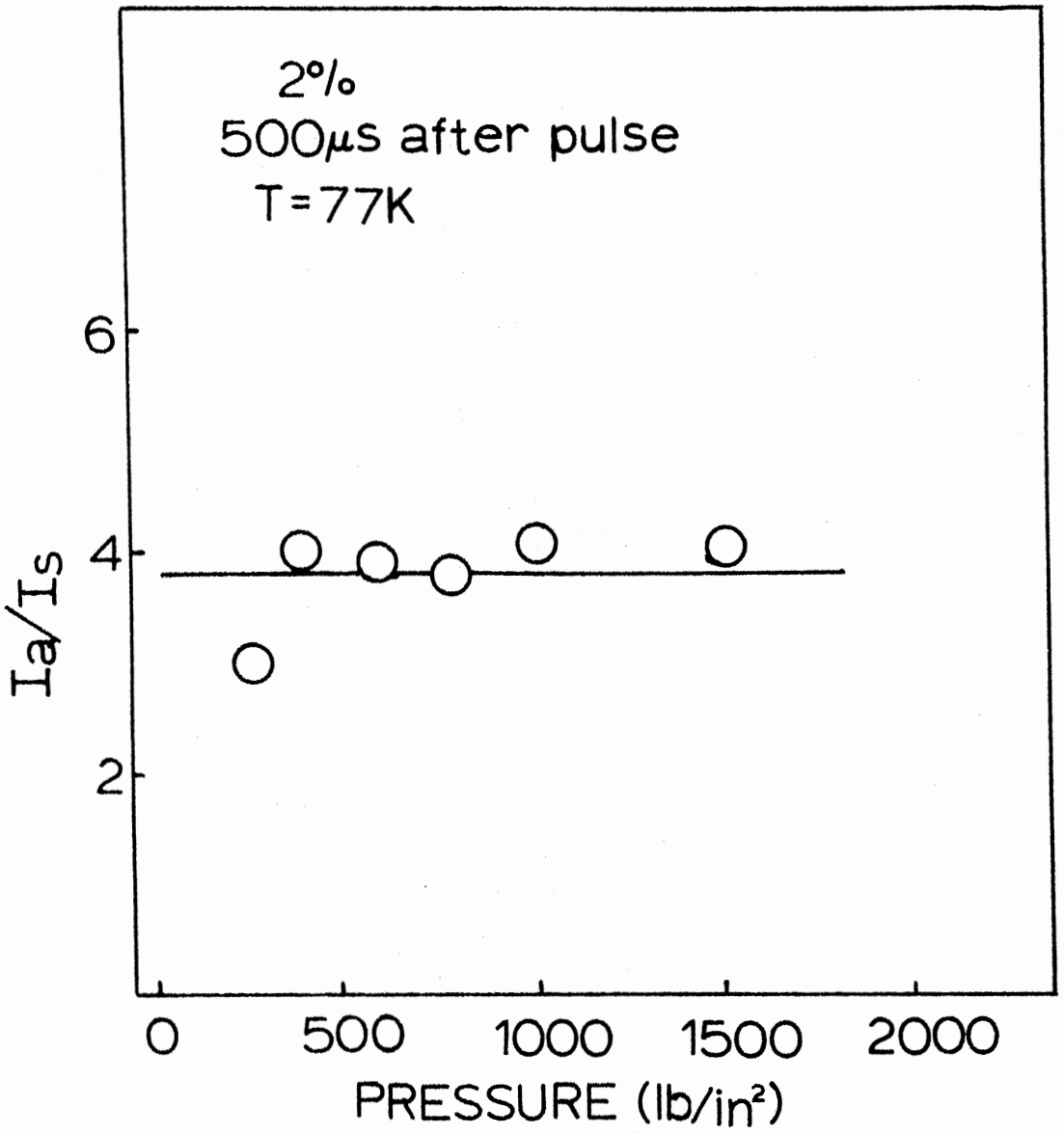

Figure 26. Effect of Uniaxial Stress on I_a/I_s

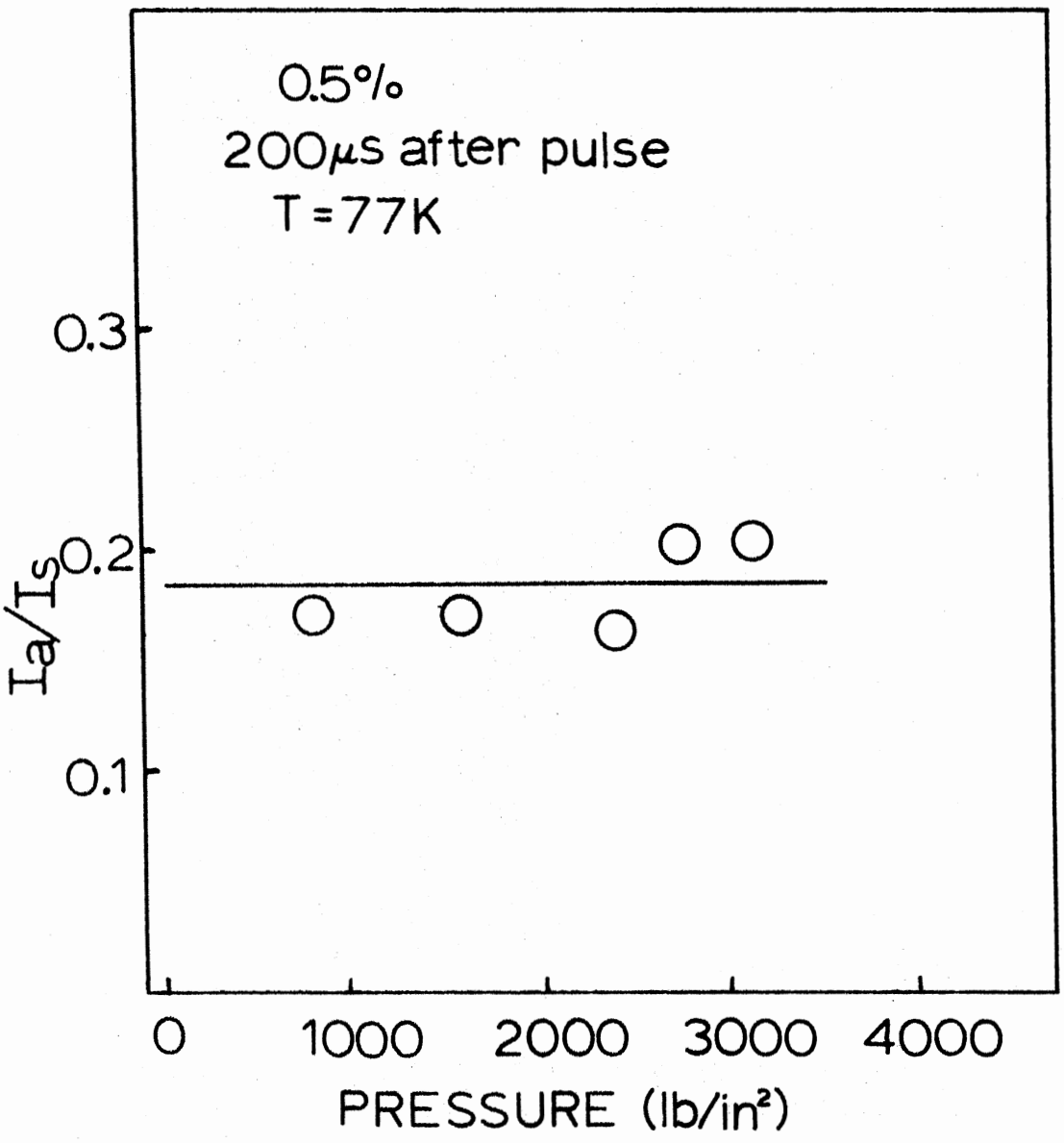

Figure 27. Effect of Uniaxial Stress on I_a/I_s

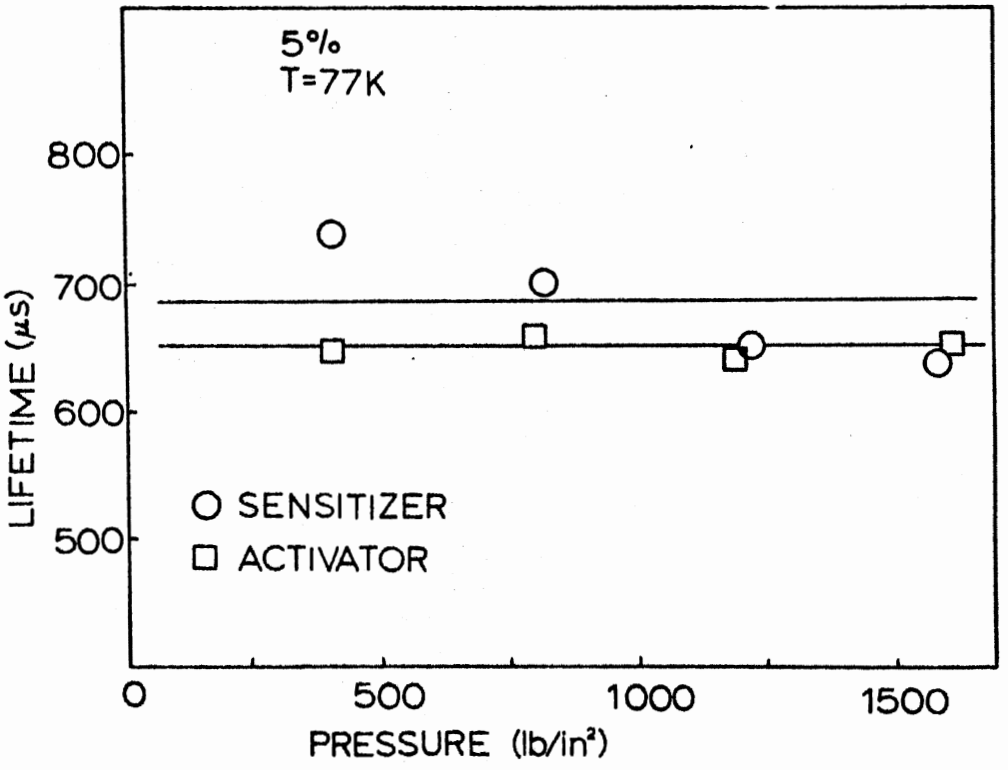

Figure 28. Effect of Uniaxial Stress on Lifetime

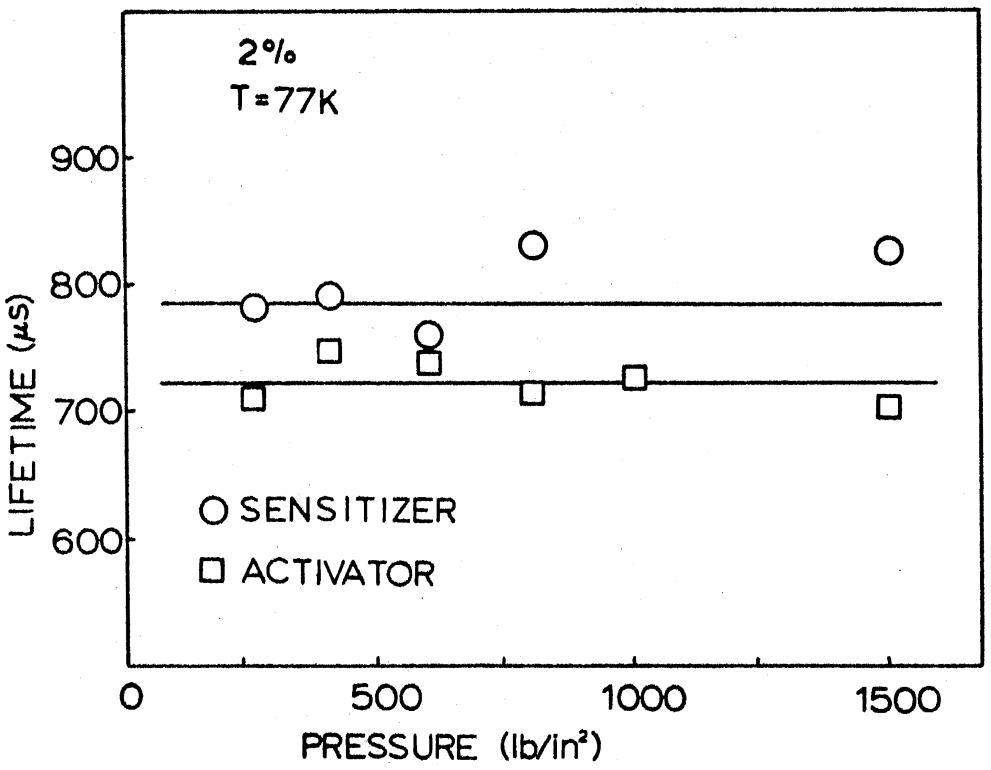

Figure 29. Effect of Uniaxial Stress on Lifetime

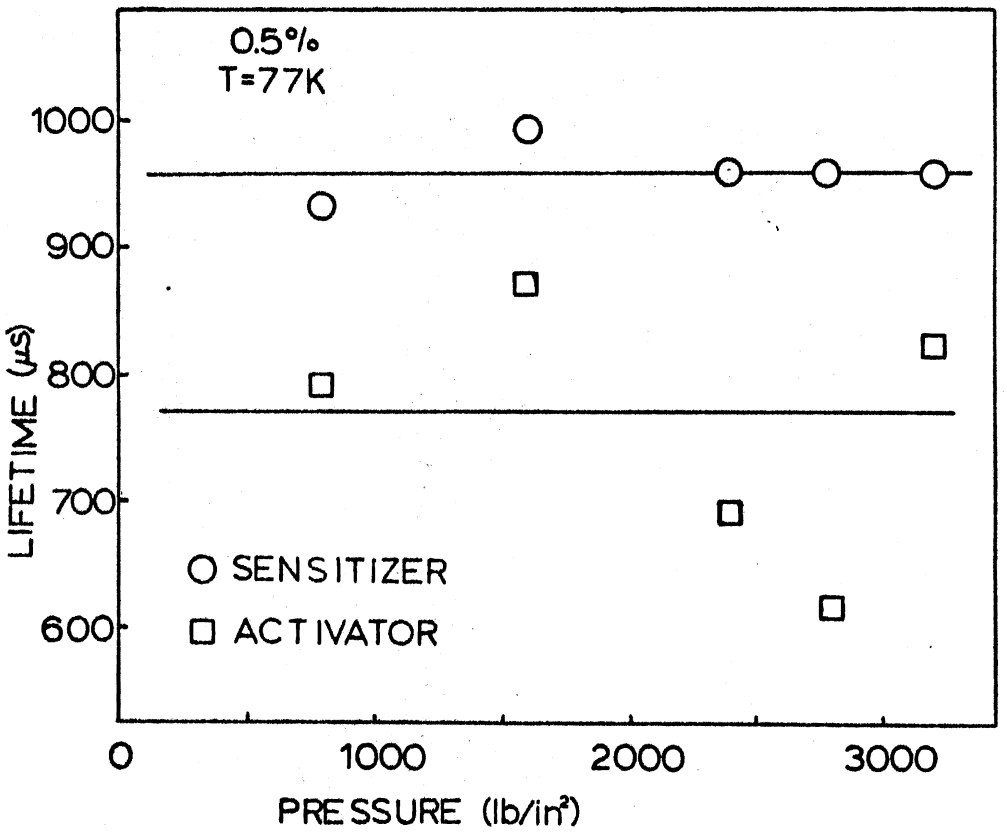

Figure 30. Effect of Uniaxial Stress on Lifetime

TABLE VIII

EFFECT OF UNIAXIAL STRESS ON I_a/I_s AND LIFETIMES

$T = 77^{o}K$	5% Sm^{3+} $\lambda_{ex} = 4020$ Å	500 μs After Pulse	
Pressure (lb/in^2)	I_a/I_s	τ_s(μs)	τ_a(μs)
400	26	742	648
800	28	698	666
1200	27	649	636
1600	32	630	649

TABLE IX

EFFECT OF UNIAXIAL STRESS ON I_a/I_s AND LIFETIMES

$T = 77^{o}K$	2% Sm^{3+} $\lambda_{ex} = 4020$ Å	500 μs After Pulse	
Pressure (lb/in^2)	I_a/I_s	τ_s(μs)	τ_a(μs)
250	3.1	797	711
400	4.1	784	752
600	3.9	755	741
800	3.8	833	717
1000	4.1	-	728
1500	4.1	822	707

TABLE X

EFFECT OF UNIAXIAL STRESS ON I_a/I_s AND LIFETIMES

$T = 77^{o}K$	0.5% Sm^{3+} $\lambda_{ex} = 4020$ Å		200 μs After Pulse
Pressure (lb/in^2)	I_a/I_s	τ_s(μs)	τ_a(μs)
800	.17	933	786
1600	.17	994	870
2400	.16	958	688
2800	.20	960	613
3200	.20	958	824

CHAPTER IV

CONCLUSIONS

Perhaps the most interesting aspect of this study is the observation that the narrow linewidth exitation used exites samarium ions in an environment which permits energy transfer and cross relaxation to occur via the exchange interaction. The results of both concentration quenching of lifetimes, and low temperature energy transfer suggest this. Hsu and Powell had previously observed an electric quadrupole-quadrupole interaction in this system with a 4 $\mathring{A}$ linewidth laser, and most other rare earth studies see, and theory predicts, an electric multipole interaction except at high concentrations where the average ion-ion separations are small.

One explanation is that samarium ions migrate at room temperatures to form clusters over a period of time. This behavior is observed in $KCl:Eu^{2+}$ but because of the close packed scheelite structure of $CaWO_4$ this is unlikely. Another possibility mentioned earlier is that the narrow line exitation preferentially exites the small number of clusters of samarium ions that would normally exist in a random distribution.

If the narrow linewidth exitation is responsible for the observation of the exchange interaction, an examination of this effect would be in order. Perhaps there is fine structure in the 4020 $\mathring{A}$ exitation peak that would explain the results. Future experiments along this line may clarify the problem.

REFERENCES

1. Dieke, G. H., Spectra and Energy Levels of Rare Earth Ions in Crystals, editors Crosswhite, H. M., Crosswhite, H. (Interscience Publishers 1961).

2. VanUitert, L. G., J. Electrochem. Soc. 114, 1048 (1967).

3. VanUitert, L. G. and L. F. Johnson, J. Chem. Phys. 44, 3514 (1966).

4. VanUitert, L. G., E. F. Dearborn, and J. J. Rubin, J. Chem. Phys. 45, 1578 (1966).

5. Kushida, T., J. Phy. Soc. Japan 34, 1318 (1973).

6. Kushida, T., J. Phys. Soc. Japan 34, 1327 (1973).

7. Kushida, T., J. Phys. Sco. Japan 34, 1334 (1973).

8. Chrysochoos, J., J. Chem. Phys. 61, 4596 (1974).

9. Hsu, C. and R. C. Powell, J. Phys. C. 9, 2467 (1976).

10. Wybourne, B. G., J. Chem. Phys. 36, 2301 (1962).

11. Rast, H. E., J. L. Fry, and H. H. Caspers, J. Chem. Phys. 46, 1460 (1967).

12. Babkina, T. V., V. F. Zolin and E. N. Muravev, Optics and Spect. (USSR) 32, 613 (1972).

13. Barker, Jr., A. S., Phys. Rev. 135, A742 (1964).

14. Russell, J. P. and R. Loudon, Proc. Phys. Soc. 85, 1029 (1965).

15. Nassau, K. J., J. Phys. Chem. Solids 24, 1511 (1963).

16. Dexter, D. L., J. Chem. Phys. 21, 836 (1953).

17. Anderson, P. W., "Exchange in Insulators: Superexchange, Direct Exchange and Double Exchange" in Magnitism, Vol 1., editors G. T. Rado and H. Suhl (Academic Press, N.Y. 1963) Chapter 2.

18. Mims, W. B. and R. Gillan, J. Chem. Phys. 47, 3518 (1967).

19. Treadaway, M. J. and R. C. Powell, Phys. Rev. B 11, 862 (1975).

20. Treadaway, M. J. and R. C. Powell, J. Chem. Phys. 61, 4003 (1974)

21. Peterson, R. G. and R. C. Powell, J. Luminescence 16, 285 (1978).

22. Axe, J. D. and P. F. Weller, J. Chem. Phys. 40, 3066 (1964).

23. Treadaway, M. J., Personal Communication (1980).

24. Förster, T., Ann. Physik 2, 55 (1948).

25. Förster, T., Z. Naturforschg 4a, 321 (1949).

26. Eisenthal, K. B. and S. Siegel, J. Chem. Phys. 41, 652 (1964).

27. Inokuti, M. and F. Hirayama, J. Chem. Phys. 43, 1978 (1965)

28. VanDerDoesDeBye, J. A. W., J. L. Sommerdijk, J. Hornstra, A. Bril and A.L.N. Stevels, J. Luminescence 18/19, 285 (1979).

29. Holstein, T., S. K. Lyo and R. Orbach, To be published.

30. Weber, M. J., Phys. Rev. B 4, 2932 (1971).

VITA

William Bryan Smith

Candidate for the Degree of

Doctor of Philosophy

Thesis: INVESTIGATION OF ENERGY TRANSFER IN SAMARIUM DOPED CALCIUM TUNGSTATE CRYSTALS USING TIME RESOLVED SITE SELECTION SPECTROSCOPY

Major Field: Physics

Biographical:

Personal Data: Born in New Orleans, Louisiana, Steptember 25, 1953.

Education: Graduated from Sheffield Village High School, Sheffield, Ohio, in 1971; received Bachelor of Science degree in Physics from Kansas State University in 1975; completed requirements for the Doctor of Philosophy degree at Oklahoma State University in December, 1980.